

Environment-Enhanced Single-Photon Absorption in a Nano-Ring of Dipole-Coupled Quantum Emitters

Eric Sánchez-Llorente,^{1,2} Helmut Ritsch,³ and Maria Moreno-Cardoner^{1,2}

¹*Departament de Física Quàntica i Astrofísica and Institut de Ciències del Cosmos, Universitat de Barcelona, Martí i Franquès 1, E-08028 Barcelona, Spain.*

²*Institut de Ciències del Cosmos, Universitat de Barcelona, Martí i Franquès 1, E-08028 Barcelona, Spain*

³*Institut für Theoretische Physik, Universität Innsbruck, Technikerstraße 21a, A-6020 Innsbruck, Austria*

(Dated: May 28, 2026)

Decoherence is mostly detrimental in quantum information and quantum optics applications. However, the interplay between environment-induced incoherent dynamics and unitary evolution can give rise to novel quantum many-body phenomena that can be harnessed as a useful resource. As is well known, in dense subwavelength atomic arrays only a single collective eigenmode in the single-excitation manifold couples strongly to free-space radiation, exhibiting superradiant spontaneous emission. Most of the remaining eigenstates form a manifold of weakly radiative modes, giving rise to long-lived subradiant excitations. Here we demonstrate that populating these subradiant modes via additional decoherence mechanisms, such as dephasing or coupling to phonons, can significantly enhance single-photon absorption in a nanoring of quantum emitters. Such nanoring geometry is particularly appealing due to its unique optical properties and its resemblance to natural light-harvesting complexes, which serve as efficient antennas in photosynthesis. Our findings may shed light on fundamental aspects of energy absorption in nature; despite the much greater complexity of biological systems, they may nonetheless operate according to similar underlying optical principles.

PACS numbers: 42.50.Ct, 42.50.Nn

I. INTRODUCTION

Structured subwavelength arrays of quantum emitters constitute a versatile platform for exploring light-matter interactions in the quantum regime [1–5]. In dense ensembles of quantum emitters, where interparticle distances are of the order of the resonant wavelength or smaller, the quantum emitters couple collectively to the same free-space vacuum modes of the electromagnetic field. This leads to coherent light-mediated dipole-dipole interactions and collective radiation processes [6–8]. This is in stark contrast to dilute ensembles, where spontaneous emission occurs independently for each emitter.

Cooperative effects in quantum optics are particularly pronounced in ordered arrays of quantum emitters, where interference between scattered fields can be engineered through geometry. The spatial arrangement of the emitters determines both the strength of coherent dipole-dipole interactions and the collective radiative response [9–13]. In subwavelength arrays, destructive interference will give rise to long-lived collective excitations with strongly suppressed radiative decay rates, commonly referred to as subradiant states [1, 11, 14, 15]. Generally, collective modes may also exhibit strongly directional emission in a preferred radiation channel while being weakly coupled to other modes of the electromagnetic field [11, 16, 17].

The existence of such subradiant and selectively radiative states has attracted considerable attention due to their potential applications in quantum technologies. Long-lived collective excitations can serve as resources for single-photon storage [11, 18, 19], the realization of coherent photon-photon interactions and qubit gates im-

plementation [20–23], efficient transport [15, 24, 25] and the enhancement of quantum metrology protocols [26, 27]. They have also been proposed as building blocks for chiral and topological quantum optics in ordered emitter arrays [28, 29]. The ability to engineer collective decay through geometry thus provides a versatile tool for quantum information processing and quantum simulation.

Importantly, geometry-engineered collective radiative states are increasingly accessible in state-of-the-art experiments. Optical tweezer arrays [30–33] and optical lattices [3, 23] now allow the assembly of ordered emitter configurations with subwavelength spacing and high positional control. Complementary platforms based on semiconductor quantum dots [34] and superconducting qubits coupled to microwave resonators [35] provide additional routes to engineer collective radiative interactions in solid-state systems. Together, these developments open realistic avenues for implementing and probing the collective phenomena discussed above.

Among the various geometries investigated, rings of quantum emitters exhibit a high degree of symmetry, which gives rise to remarkable collective optical properties [15, 36]. Owing to their rotational symmetry, ring configurations naturally support collective excitations with well-defined angular momentum. Some of these modes exhibit strongly suppressed coupling to free-space radiation, resulting in highly subradiant states, while others form optically confined modes that resemble cavity-like resonances. Beyond their interest in atomic and solid-state implementations, such ring structures closely resemble natural light-harvesting complexes, including the LH1 and LH2 complexes in purple bacteria [37, 38]. This analogy has triggered to engineer

biomimetic devices designed for efficient light absorption, excitation transport, and sensing [25, 36, 39–42].

In practice, real world implementations inevitably involve additional sources of decoherence beyond radiative decay. In particular, coupling to environmental degrees of freedom leads to pure dephasing and thermal fluctuations, which can significantly modify the lifetime and coherence of collective excitations. In atomic systems, such effects may originate from motional fluctuations [43], while in solid-state platforms (including superconducting qubits) they can arise from fluctuations of the electromagnetic environment. In biomimetic contexts, environmental interactions emulate the protein scaffold surrounding chromophores in organic complexes [37, 44].

Decoherence is often regarded as a detrimental effect that limits quantum applications. Yet, when combined with collective radiative phenomena, decoherence can acquire a constructive role. As we shall see, controlled dephasing can redistribute population among collective eigenmodes, enhancing the effective coupling to radiatively protected or efficiently absorbing channels [40]. This interplay can enable directional excitation transport and, more importantly for the present work, enhance single-photon absorption. These considerations suggest that environmental noise, rather than merely degrading coherence, may be harnessed to optimize light–matter interactions in collective systems.

Motivated by this perspective, we present a systematic study of the interplay between collective radiance and nonradiative decoherence in the process of single-photon absorption by subwavelength rings of quantum emitters. Using the absorption cross section as our central figure of merit, we determine the regimes in which dephasing enhances absorption efficiency and quantify how this enhancement scales with system size and interparticle spacing. Our results demonstrate that collective radiation, when combined with controlled environmental noise, can improve absorption beyond the case of pure coherent dynamics.

The paper is organized as follows. In Sec. II, we introduce the model and define the main quantities of interest, including the absorption cross section. In Sec. III, we derive analytical expressions for a single emitter, which serve as a benchmark for the collective response. Sections IV and V analyze the effects of pure and thermal dephasing, respectively, for a nanoring of quantum emitters driven by coherent light in the Dicke limit, corresponding to ring sizes much smaller than the resonant wavelength. In Sec. VI we go beyond this limit and examine finite-size effects. In Sec. VII we consider the case of incoherent illumination. Finally, in Sec. VIII, we summarize our main findings.

II. MODEL AND DEFINITIONS

We consider a regular polygon (from now on nanoring) of N identical two-level quantum emitters trapped at

fixed position in the deep subwavelength regime, *i.e.*, the interparticle distances are smaller than the light wavelength λ_0 associated with the emitters transition frequency $\omega_0 = ck_0$, being $k_0 = 2\pi/\lambda_0$ the corresponding wave-number. The emitters feature electric dipole moments $\boldsymbol{\wp}_i$ ($i = 1, \dots, N$), with $|\boldsymbol{\wp}_i| = \wp$. The distance between two nearest neighbours is denoted by d (see Fig. 1). Throughout this work, we mostly restrict to the case where atoms are transversally polarized to the plane containing the ring. A different dipole orientation can be easily taken into account within the theoretical framework that is introduced later, but it modifies the dispersion relation and the sorting of eigenstates in energy, changing the light absorption efficiency under certain mechanisms, as it will be described later.

For interparticle separations comparable to or smaller than the resonant wavelength, the emitters couple to common modes of the electromagnetic vacuum, giving rise to coherent dipole–dipole interactions and collective spontaneous emission. Within the Born–Markov approximation, which is appropriate for many quantum optical platforms, the system dynamics are described by a Lindblad master equation of the form ($\hbar = 1$):

$$\dot{\rho} = -i[\hat{H}, \rho] + \mathcal{L}[\rho]. \quad (1)$$

In the absence of additional noise or relaxation channels, the coherent and dissipative parts are entirely determined by the vacuum-mediated dipole–dipole coupling, $\hat{H} = \hat{H}_{\text{dd}}$ and $\mathcal{L} = \mathcal{L}_{\text{dd}}$. The coherent contribution is given by

$$\hat{H}_{\text{dd}} = \sum_{i \neq j} J_{ij} \hat{\sigma}_i^{eg} \hat{\sigma}_j^{ge}, \quad (2)$$

while the collective radiative decay is described by [7]:

$$\mathcal{L}_{\text{dd}}[\rho] = \frac{1}{2} \sum_{i,j} \Gamma_{ij} (2\hat{\sigma}_j^{ge} \rho \hat{\sigma}_i^{eg} - \{\hat{\sigma}_i^{eg} \hat{\sigma}_j^{ge}, \rho\}) \quad (3)$$

Here $\hat{\sigma}_j^{ge}$ ($\hat{\sigma}_j^{eg}$) is the lowering (raising) operator between excited and ground state of emitter j . The dispersive and dissipative couplings are given, respectively, by $J_{ij} = \hat{\boldsymbol{\wp}}_i^* \cdot \text{Re} \mathbf{G}_{ij} \cdot \hat{\boldsymbol{\wp}}_j$ and $\Gamma_{ij} = -2\hat{\boldsymbol{\wp}}_i^* \cdot \text{Im} \mathbf{G}_{ij} \cdot \hat{\boldsymbol{\wp}}_j$, with $\hat{\boldsymbol{\wp}}_i = \boldsymbol{\wp}_i / \wp$ the dipole orientation of the i -th atom. Here \mathbf{G}_{ij} is given by the free space Green’s tensor,

$$\mathbf{G}_{ij} = \frac{3\Gamma_0}{4} \frac{e^{ik_0 r}}{k_0^3 r^3} \times \left[(1 - ik_0 r - k_0^2 r^2) \mathbb{I} + (-3 + 3ik_0 r + k_0^2 r^2) \frac{\mathbf{r} \otimes \mathbf{r}}{r^2} \right]. \quad (4)$$

In this expression, $\mathbf{r} = \mathbf{r}_i - \mathbf{r}_j$ is the vector connecting dipoles i and j , whose modulus is denoted by $r = |\mathbf{r}|$, and $\Gamma_0 = \wp^2 k_0^3 / 3\pi\epsilon_0$ is the spontaneous emission rate of a single emitter. For the case considered in this work, of dipoles oriented transversally to the ring plane, only the zz component of the tensor is relevant, simplifying into $G_{ij}^{zz} = 3\Gamma_0 e^{ik_0 r} (1 - ik_0 r - k_0^2 r^2) / 4k_0^3 r^3$.

The system discussed above is illuminated by coherent light (such as a laser) of very weak intensity and frequency ω . This can be modeled by adding to \hat{H} in Eq.(1) the term $\hat{H}_{\text{in}} = -\sum_i (\Omega_i \hat{\sigma}_i^{eg} + \text{h.c.}) - \delta \sum_i \hat{\sigma}_i^{ee}$, with Rabi frequency $\Omega_i \equiv \wp \cdot E^+(\mathbf{r}_i)/\hbar$ and $E^+(\mathbf{r}_i) = \langle \hat{E}^+(\mathbf{r}_i) \rangle$ the amplitude of the coherent field, that we consider a plane wave of the form $\hat{E}(\mathbf{r}, t) = \hat{E}^+(\mathbf{r})e^{-i\omega t} + \hat{E}^-(\mathbf{r})e^{i\omega t}$. Here $\delta = \omega - \omega_0$ denotes the detuning between the external drive frequency ω and the atomic transition frequency ω_0 .

Collective eigenmodes in a nano-ring of quantum emitters.— When the atoms are illuminated by a very weak external field, the dynamics of the system are mostly restricted to the ground state and single excitation manifold, while the population in higher excitation manifolds is negligible.

With this assumption the term $\hat{\sigma}_j^{ge} \rho \hat{\sigma}_i^{eg}$ in Eq. (3) can be neglected and the Lindblad master equation corresponding to the dipole-dipole interactions can be written as

$$\dot{\rho} = -i \left(\hat{H}_{\text{eff}} \rho - \rho \hat{H}_{\text{eff}}^\dagger \right), \quad (5)$$

where $\hat{H}_{\text{eff}} = \sum_{ij} (J_{ij} - i\Gamma_{ij}/2) \hat{\sigma}_i^{eg} \hat{\sigma}_j^{ge}$ is a non-hermitian effective Hamiltonian. In this single excitation sector, the eigenstates of \hat{H}_{eff} decay with well defined rate into the ground state, and represent a proper collective basis to describe the dynamics of the system. For the nano-ring geometry considered here, displaying discrete rotational symmetry, collective eigenmodes correspond to spin-waves of the form:

$$|m\rangle = \frac{1}{\sqrt{N}} \sum_{j=1}^N e^{i2\pi m j/N} |j\rangle, \quad (6)$$

with $|j\rangle = \hat{\sigma}_j^{eg} |g\rangle$ and well defined angular momentum value $m = 0, \pm 1, \pm 2, \dots, [\pm(N-1)/2]$, being $[\cdot]$ the ceiling function. The corresponding collective frequency shifts and decay rates, are then just given by the Fourier transform functions

$$\tilde{J}_m = \sum_{\ell=j-k} e^{i2\pi m \ell/N} J_{jk}, \quad (7)$$

$$\tilde{\Gamma}_m = \sum_{\ell=j-k} e^{i2\pi m \ell/N} \Gamma_{jk}. \quad (8)$$

In this work we focus on a nanoring of quantum emitters transversally polarized with respect to the plane containing the ring. In the first sections, we will restrict to the deep subwavelength regime (*i.e.*, $d/\lambda \ll 1$), also known as the Dicke limit, where the effective Hamiltonian acquires a particularly simple form:

$$\hat{H}_{\text{eff}} = J \sum_j (\hat{\sigma}_j^{eg} \hat{\sigma}_{j+1}^{ge} + \hat{\sigma}_j^{ge} \hat{\sigma}_{j+1}^{eg}) - i \frac{\Gamma_0}{2} \sum_{i,j} \hat{\sigma}_i^{eg} \hat{\sigma}_j^{ge}. \quad (9)$$

The short-range behavior of the dispersive couplings J_{ij} with interparticle distance ($\propto r_{ij}^{-3}$) leads to a coherent term in the Hamiltonian Eq.(9) that reduces to the tight-binding model, where only first-neighbour couplings are non-zero. This leads to a dispersion relation of the form

$$\tilde{J}_m = J \cos(2\pi m/N), \quad (10)$$

with $J = 3\Gamma_0/2k_0^3 d^3 > 0$. For positive J , the fully symmetric mode $m = 0$ corresponds to the maximum of the band and therefore lies highest in energy. In contrast, the dissipative term contains identical couplings between any pair of emitters, and thus, there exists only a single bright mode corresponding to $m = 0$, with decay rate $N\Gamma_0$, and $N - 1$ states that are dark with $\tilde{\Gamma}_m \approx 0$. As it will be detailed later, this specific order of the states, with a bright mode higher in energy, is crucial to exploit the global thermal bath mechanism for light absorption.

Light Absorption Efficiency.— To maximize light scattering, we choose the frequency of the external drive ω in resonance with the single bright mode described before, *i.e.*, $\omega = \tilde{J}_{m=0}$. Strictly in the Dicke limit, where the remaining modes are perfectly dark, this is the only mode that couples to light.

In order to model light absorption in the system, we add an irreversible decay channel into an additional trapping state (t), acting as a sink or energy extractor. The role of this state is only to accumulate excitations that are not scattered into free space, and thus, it does not directly contribute to the dynamics of the remaining degrees of freedom. This additional channel is modeled as an additional dissipator contributing to \mathcal{L} and defined as:

$$\mathcal{L}_{\text{T}}[\rho] = \Gamma_{\text{T}} \sum_j \left(\hat{\sigma}_j^{te} \rho \hat{\sigma}_j^{et} - \frac{1}{2} \{ \hat{\sigma}_j^{ee}, \rho \} \right), \quad (11)$$

where $\hat{\sigma}_j^{te}$ ($\hat{\sigma}_j^{et}$) are now the lowering (raising) operator between excited state of emitter j and trapping state. For simplicity, we assume that all sites have the same irreversible decay rate into this state, but a generalization of this model to a site-dependent value of Γ_{T} is straightforward.

Within this model, we quantify the light absorption efficiency through the absorption cross-section. The absorption cross-section per unit beam area defines the probability that an incident photon is absorbed, $\sigma_{\text{abs}}/A = \dot{n}_{\text{abs}}/\dot{n}_{\text{in}}$, where $\dot{n}_{\text{abs}} = \Gamma_{\text{T}} \rho_{ee}$ and \dot{n}_{in} denote the rates of absorbed and incident photons, respectively. It is convenient to express the absorption cross section in units of the single-emitter scattering cross section $\sigma = 6\pi/k_0^2$. Dividing σ by the beam area similarly yields the probability that an incident photon is scattered by a single emitter, $\sigma/A = \dot{n}_{\text{sc}}/\dot{n}_{\text{in}}$, where \dot{n}_{sc} is the single emitter scattering rate. For a plane wave, the incident photon rate per unit area is obtained by dividing the energy flux (energy per unit time and area) by the photon energy, which gives $\dot{n}_{\text{in}} = 4|\Omega|^2 A/\sigma\Gamma_0$. Combining these

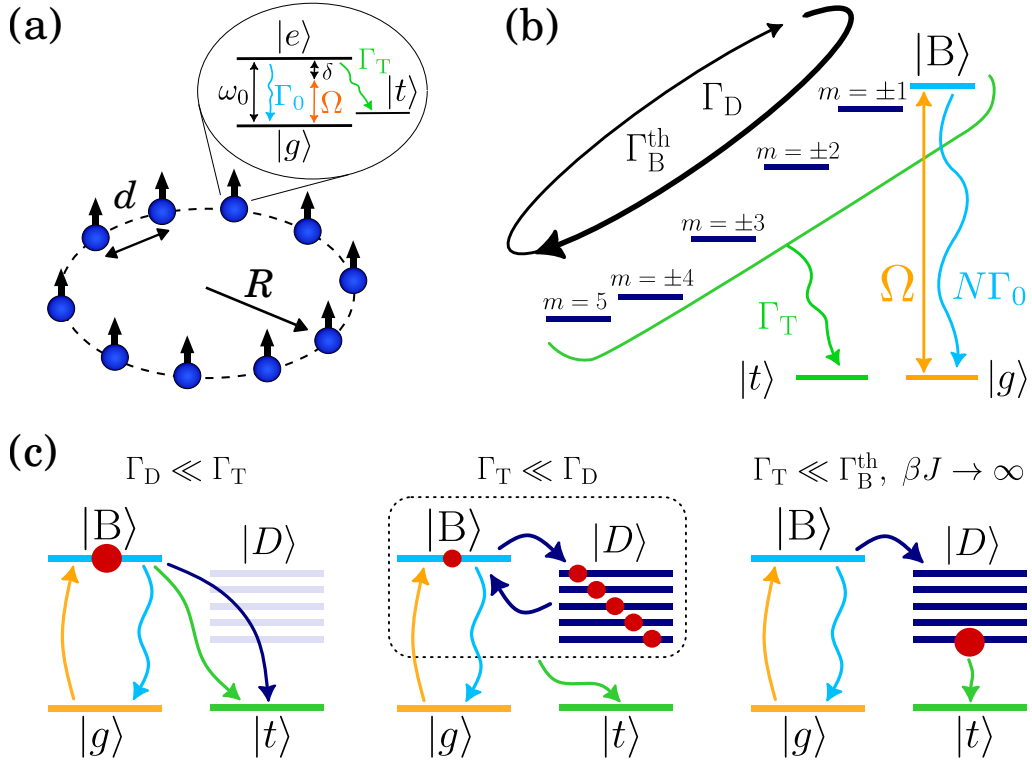


FIG. 1. **(a)** Schematic of the system. A nanoring of three-level quantum emitters ($|g\rangle$, $|e\rangle$ and $|t\rangle$) with radius R and interparticle spacing d , coupled through dipole–dipole interactions and driven by a classical field. Black arrows indicate the dipole moments; Ω and δ denote the Rabi frequency and detuning of a coherent drive. An emitter can decay from $|e\rangle$ into $|g\rangle$ by spontaneously emitting photons at rate Γ_0 , while it irreversibly decays into $|t\rangle$ at rate Γ_T . **(b)** Level scheme of the single-excitation collective modes of the nano-ring, in the small-volume (Dicke) limit ($R/\lambda_0 \ll 1$). The bright mode (B) and the ground state (g) are coherently coupled by the external drive. Local and thermal dephasing, with rates Γ_D and Γ_B^{th} , respectively, redistribute population among collective modes. **(c)** Population redistribution in the limiting regimes discussed in the main text. For $\Gamma_D \ll \Gamma_T$ (or $\Gamma_B^{\text{th}} \ll \Gamma_T$) the excitation remains primarily in the bright mode, and the system behaves as a single emitter with irreversible decay rate $\Gamma_T + \Gamma_D$. For $\Gamma_T \ll \Gamma_D$ the population is uniformly distributed among collective modes, effectively reducing the radiative decay to $|g\rangle$ by a factor N . In the thermal dephasing case, for $\Gamma_T \ll \Gamma_B^{\text{th}}$ and $\beta J \rightarrow \infty$, the population concentrates in the darkest mode, leading to a maximal absorption for any $\Gamma_T \leq N\Gamma_0$.

expressions we obtain:

$$\frac{\sigma_{\text{abs}}}{\sigma} = \frac{\Gamma_T \Gamma_0}{4|\Omega|^2} \rho_{ee}. \quad (12)$$

In the following, we focus on the steady-state solution and denote the excited-state population by ρ_{ee}^{st} .

Decoherence mechanisms.— The main goal of the work is to analyse when the interplay between collective spontaneous emission and dephasing gives rise to an enhanced single photon absorption efficiency. We compare the effect of two different decoherence mechanisms: pure and thermal dephasing. The dynamics described by the two models naturally arises when the electronic excitations are coupled to an external phononic bath (see Appendix A for a full derivation of the model). Physically, these mechanisms are expected to be present, for instance, in systems of natural light harvesting complexes, arising due to molecular vibrations, or in artificial systems of quantum dots, as a consequence of

residual electromagnetic field noise.

• **Pure local dephasing model:** We add the dissipator \mathcal{L}_D to the Lindblad \mathcal{L} in Eq.(1):

$$\mathcal{L}_D[\rho] = \Gamma_D \sum_j \left(\hat{\sigma}_j^{ee} \rho \hat{\sigma}_j^{ee} - \frac{1}{2} \{ \hat{\sigma}_j^{ee}, \rho \} \right). \quad (13)$$

For a N -fold rotationally symmetric ring, as the one considered here, it is straightforward to show that the Lindblad \mathcal{L}_D acts on the collective eigenmodes basis states Eq.(6) as:

$$\begin{aligned} \dot{\rho}_{mm'} &= \langle m | \mathcal{L}_D[\rho] | m' \rangle = \Gamma_D \left[\frac{\rho_{ee}}{N} \delta_{m,m'} - \rho_{mm'} \right], \\ \dot{\rho}_{mg} &= \langle m | \mathcal{L}_D[\rho] | g \rangle = -\frac{\Gamma_D}{2} \rho_{mg}. \end{aligned} \quad (14)$$

Here $\rho_{mm'} = \langle m | \rho | m' \rangle$ describes the collective state populations or coherences, depending if $m' = m$ or $m \neq m'$, respectively, and $\rho_{mg} = \langle m | \rho | g \rangle$. Therefore, Eq. (14)

describes the effect of local dephasing as an exchange of population between different collective states, and a suppression of all coherences (between different excited states and also with the ground state). Then, it is clear that if only this mechanism is present, the excited state density matrix components evolve towards a maximally mixed state, with all collective modes equally populated, *i.e.*, $\rho_{mm} = \rho_{ee}/N$ ($m = 1, \dots, N$).

• **Thermal dephasing model:** A different mechanism is the coupling with a global thermal bath, with which the system can exchange phonon-like excitations [37, 44–48]. The corresponding dissipator can be written as

$$\mathcal{L}_{\text{th}}[\rho] = \sum_{m,m'} k_{m \rightarrow m'} \left(\hat{\sigma}_{m'}^{eg} \hat{\sigma}_m^{ge} \rho \hat{\sigma}_m^{eg} \hat{\sigma}_{m'}^{ge} - \frac{1}{2} \{ \hat{\sigma}_m^{eg} \hat{\sigma}_m^{ge}, \rho \} \right), \quad (15)$$

where the indices m and m' run over all possible collective eigenmodes defined in Eq. (6) and $\hat{\sigma}_m^{eg} \equiv \sum_j \langle j|m \rangle \hat{\sigma}_j^{eg}$ ($\hat{\sigma}_m^{ge}$) represent the creation (annihilation) operators of an excitation in mode m . These dissipator contributes then to each of the density components as:

$$\begin{aligned} \dot{\rho}_{mm'} &= \langle m | \mathcal{L}_{\text{th}}[\rho] | m' \rangle \\ &= \delta_{mm'} \sum_b k_{b \rightarrow m} \rho_{bb} - \frac{1}{2} \sum_b (k_{m \rightarrow b} + k_{m' \rightarrow b}) \rho_{mm'} \end{aligned} \quad (16)$$

$$\dot{\rho}_{mg} = \langle m | \mathcal{L}_{\text{th}}[\rho] | g \rangle = -\frac{1}{2} \sum_b k_{m \rightarrow b} \rho_{mg}. \quad (17)$$

The transition rate from mode a to mode b is defined as:

$$k_{a \rightarrow b} \equiv n(\omega_{ba}) \mathcal{J}(\omega_{ba}) + (1 + n(\omega_{ab})) \mathcal{J}(\omega_{ab}), \quad (18)$$

with $\omega_{ba} = \tilde{J}_b - \tilde{J}_a$ the energy difference between the collective modes b and a , $n(\omega) = (e^{\beta\omega} - 1)^{-1}$ is the mean number of phonons with frequency ω following the Bose-Einstein distribution with inverse temperature β , and $\mathcal{J}(\omega)$ is the spectral density of the bath, which is given by the density of phonon modes weighted by the coupling strength with the system, at frequency ω .

Following previous work [37, 47, 49], we will adopt here a spectral function of the Drude-Lorentz form

$$\mathcal{J}(\omega) = \frac{2f\omega_c}{\omega^2 + \omega_c^2} \omega, \quad (19)$$

and restrict to the Ohmic regime for which the function becomes linear with ω , $\mathcal{J}(\omega) \approx \bar{f}\omega$, with $\bar{f} = 2f/\omega_c$. This approximation is valid assuming that all frequencies involved in the problem are smaller than the cut-off frequency ω_c . More refined models, which depend sensitively on the molecular composition and environment [50], can be employed to describe realistic light-harvesting complexes. However, we expect that the main

conclusions of this work are robust with respect to the specific form of the environmental spectral density.

If only thermal dephasing is present in the dissipator, the steady state populations fulfill the detailed balance condition $\rho_{aa}/\rho_{bb} = k_{a \rightarrow b}/k_{b \rightarrow a}$, which for a spectral density such that $\mathcal{J}(\omega) = -\mathcal{J}(-\omega)$, implies the thermal state with populations $\rho_{aa}/\rho_{bb} = e^{-\beta\omega_{ab}}$.

In the high temperature limit ($\beta \rightarrow 0$), where the rate $k_{a \rightarrow b} \approx 2\bar{f}/\beta = k$ becomes independent of ω_{ab} , the state corresponds to a maximally mixed state, with equal population in each collective mode. We note that in this case, Eq. (16) becomes formally equivalent to the population dynamics Eq. (14) for the pure dephasing case, when identifying $k = \Gamma_D/N$.

In the opposite limit of very low temperature ($\beta \rightarrow \infty$) the rate can be written as $k_{a \rightarrow b} = 2\bar{f}\text{ReLU}(\omega_{ab})$, with $\text{ReLU}(x)$ the rectified linear unit function, being equal to x for positive inputs and 0 otherwise. Thus, the rate is non-zero and linear with ω_{ab} for a decreasing energy transition $|a\rangle \rightarrow |b\rangle$, while it is exactly zero for a transition that implies an increase in energy. The thermal Liouvillian then drives the excited state density matrix components into a statistical mixture where only the lowest energy collective state is populated.

III. SINGLE-EMITTER ABSORPTION

In this section we provide analytical expressions for a single atom which will be used later as a benchmark for the multi-atom case with collective scattering. We consider an atom that couples to light with an electric dipole moment \wp and decays to the ground and trapping states with rates Γ and Γ_T , respectively. The atom is driven by a coherent resonant field with Rabi frequency Ω .

The reduced density matrix of the emitter evolves according to the following set of differential equations:

$$\dot{\rho}_{gg} = \Gamma \rho_{ee} + i(\Omega^* \rho_{eg} - \Omega \rho_{ge}), \quad (20a)$$

$$\dot{\rho}_{ge} = -\frac{1}{2}(\Gamma + \Gamma_T + \Gamma_D) \rho_{ge} + i\Omega^*(\rho_{ee} - \rho_{gg}), \quad (20b)$$

$$\dot{\rho}_{ee} = -(\Gamma + \Gamma_T) \rho_{ee} + i(\Omega \rho_{ge} - \Omega^* \rho_{eg}). \quad (20c)$$

We find the excited state by setting the time derivatives to be zero ($\dot{\rho}_{ee} = \dot{\rho}_{ge} = 0$) [51]. We focus in the regime of a very weak driving field ($|\Omega|/\Gamma_0 \ll 1$), where we can approximate $\rho_{gg}^{\text{st}} = 1 - O(|\Omega|^2) \approx 1$. Plugging this into Eq. (20b) we readily find that

$$\rho_{ee}^{\text{1at,st}}(\Gamma) = \frac{4|\Omega|^2}{\Gamma + \Gamma_D + \Gamma_T} \cdot \frac{1}{\Gamma + \Gamma_T}, \quad (21)$$

which leads to the scattering and absorption cross-sections:

$$\frac{\sigma_{\text{sc}}^{\text{1at}}(\Gamma)}{\sigma} = \frac{\Gamma}{\Gamma + \Gamma_D + \Gamma_T} \cdot \frac{\Gamma}{\Gamma + \Gamma_T}, \quad (22)$$

$$\frac{\sigma_{\text{abs}}^{\text{1at}}(\Gamma)}{\sigma} = \frac{\Gamma}{\Gamma + \Gamma_D + \Gamma_T} \cdot \frac{\Gamma_T}{\Gamma + \Gamma_T}. \quad (23)$$

Interestingly, these expressions can be interpreted as the product of two probabilities. The first term represents the relative excitation probability, i.e., the probability that the atom is promoted from the ground to the excited state in the presence of dephasing and trapping, normalized to the case without these additional decay channels. The second term corresponds to the probability that, once excited, the atom decays through a given channel – either by spontaneous emission back to the ground state (σ_{sc}) or into the trapping state (σ_{abs}). In this picture, the two decay pathways, with rates Γ and Γ_T , define branching ratios determined by their relative weights with respect to the total decay rate $\Gamma + \Gamma_T$. In the absence of trapping and dephasing, the standard result $\sigma_{sc} = \sigma$ is recovered, as expected.

The absorption cross section of a single emitter with radiative decay rate Γ_0 is shown in Fig. 2(a) as a function of the dimensionless parameters Γ_T/Γ_0 and Γ_D/Γ_0 . As follows from Eq. (23), dephasing always reduces the absorption cross section, since it only acts to suppress the excitation probability. This behavior changes qualitatively in the multi-atom scenario, where emitters couple collectively to the electromagnetic field. As we demonstrate below, in that regime dephasing can instead enhance absorption. This contrast between independent and collective coupling constitutes one of the central results of this work.

On the other hand, σ_{abs} vanishes trivially for $\Gamma_T = 0$, since no trapping channel is available. It also tends to zero in the opposite limit $\Gamma_T \rightarrow \infty$, where strong coupling to the environment suppresses coherent excitation dynamics via the quantum Zeno effect. The absorption cross section therefore reaches its maximum value, $\sigma_{abs}^{max} = \sigma/4$, at an intermediate point where the two decay rates are equal, $\Gamma_T = \Gamma_0$. At this optimal point, excitation of the atom is still efficient while the branching ratio toward the trapping channel is maximized.

IV. COLLECTIVE ABSORPTION UNDER PURE LOCAL DEPHASING

We now consider a nano-ring with N atoms in the Dicke (small-volume) limit previously discussed ($d, R \ll \lambda_0$). When illuminating the atoms with a coherent drive, light will only couple to the bright mode. In this case, in absence of dephasing ($\Gamma_D = 0$) the system behaves as a single atom with decay rates $N\Gamma_0$ and Γ_T , and absorption cross-section identical to $\sigma_{abs}^{1at}(N\Gamma_0)$ given by Eq. (23). However, dephasing modifies σ_{abs} in an ensemble of many atoms collectively radiating.

The reduced density matrix of the emitters evolves ac-

cording to the following set of differential equations:

$$\dot{\rho}_{gg} = N\Gamma_0 \rho_{BB} + i\sqrt{N}(\Omega^* \rho_{Bg} - \Omega \rho_{gB}), \quad (24a)$$

$$\begin{aligned} \dot{\rho}_{gB} = & [-i(\tilde{J}_B - \delta) - (N\Gamma_0 + \Gamma_T + \Gamma_D)/2]\rho_{gB} \\ & + i\sqrt{N}\Omega^*(\rho_{BB} - \rho_{gg}), \end{aligned} \quad (24b)$$

$$\begin{aligned} \dot{\rho}_{BB} = & -(N\Gamma_0 + \Gamma_D + \Gamma_T)\rho_{BB} + \Gamma_D \rho_{ee}/N \\ & + i\sqrt{N}(\Omega \rho_{gB} - \Omega^* \rho_{Bg}), \end{aligned} \quad (24c)$$

$$\dot{\rho}_{DD} = -(\Gamma_D + \Gamma_T)\rho_{DD} + (N-1)\Gamma_D \rho_{ee}/N. \quad (24d)$$

Here B denotes the bright mode, while $D = \{1, \dots, N-1\}$ refers to any of the possible remaining $N-1$ perfectly dark modes, so that $\rho_{ee} = \rho_{BB} + \sum_{D=1}^{N-1} \rho_{DD}$ is the total excited state population. Similarly as in Sec. III, we find σ_{abs} for the steady state when the array is illuminated by a weak driving field ($|\Omega|/\Gamma_0 \ll 1$) and solve the equations imposing $\dot{\rho}_{Bg} = \dot{\rho}_{BB} = \dot{\rho}_{DD} = 0$ ($D = \{1, \dots, N-1\}$) [51].

Again, we approximate $\rho_{gg} = 1 - \mathcal{O}(|\Omega|^2/\Gamma_0^2) \approx 1$ in the dynamical equations. Unless otherwise stated, we consider the external drive to be resonant with the bright mode, $\delta = \tilde{J}_B$, where absorption is maximized.

Under these conditions, the steady-state equations reduce to the algebraic relations:

$$(N\Gamma_0 + \Gamma_D + \Gamma_T)\rho_{BB} - \frac{\Gamma_D}{N}\rho_{ee} = \frac{4N|\Omega|^2}{\Gamma_B^{tot}}, \quad (25a)$$

$$(\Gamma_D + \Gamma_T)\rho_{DD} - \frac{\Gamma_D}{N}\rho_{ee} = 0, \quad (25b)$$

from which the branching ratios are obtained as $\rho_{BB}/\rho_{ee} = (\Gamma_T + \Gamma_D/N)/(\Gamma_T + \Gamma_D)$ and $\rho_{DD}/\rho_{ee} = (\Gamma_D/N)/(\Gamma_T + \Gamma_D)$. It is straightforward to find the excited steady state population:

$$\rho_{ee} = \frac{4N|\Omega|^2}{N\Gamma_0 + \Gamma_D + \Gamma_T} \cdot \frac{\Gamma_D + \Gamma_T}{\Gamma_T(N\Gamma_0 + \Gamma_D + \Gamma_T) + \Gamma_D\Gamma_0}. \quad (26)$$

To understand the effect of dephasing in the dynamics, it is instructive to analyze first the limiting cases of $\Gamma_D \gg \Gamma_T$ and $\Gamma_D \ll \Gamma_T$.

Case $\Gamma_T \ll \Gamma_D$. – In the absence of trapping ($\Gamma_T = 0$) and for $\mathcal{L} = \mathcal{L}_D$, all collective modes are equally populated in the steady state (see sketch in Fig. 1(c)). In this situation, only a single bright mode decays to the ground state at an enhanced rate $N\Gamma_0$, while the remaining $N-1$ dark modes are nonradiative. As a result, the total decay is carried exclusively by the bright component, yielding an average decay rate per atom equal to Γ_0 , that is, a factor of N smaller than in the case without dephasing. Thus, we find that in steady state the excited-state population is enhanced by a factor of N compared to a single atom with decay $N\Gamma_0$, i.e., $\rho_{ee}^{st} = N\rho_{ee}^{1at,st}$, being $\rho_{ee}^{1at,st} = 4N|\Omega|^2/(N\Gamma_0 + \Gamma_D)N\Gamma_0$.

In presence of a very small trapping rate ($\Gamma_T/\Gamma_D \ll 1$)

we find an enhanced absorption cross section:

$$\frac{\sigma_{\text{abs}}}{\sigma} \Big|_{\Gamma_{\text{T}} \ll \Gamma_{\text{D}}} = \frac{N\Gamma_0}{N\Gamma_0 + \Gamma_{\text{D}} + \Gamma_{\text{T}}} \cdot \frac{\Gamma_{\text{T}}}{\Gamma_0 + \Gamma_{\text{T}}}. \quad (27)$$

While the first factor in the previous expression associated with the scattering probability is exactly the same as for the single atom case (decaying with $N\Gamma_0$), the second factor, associated with the absorption probability once an atom is excited is enhanced, as there are now N collective modes decaying irreversibly into (t). In the limit $\Gamma_{\text{T}}/\Gamma_{\text{D}} \rightarrow 0$, this leads to $\sigma_{\text{abs}} = N\sigma_{\text{abs}}^{\text{lat}}(N\Gamma_0)$.

Case $\Gamma_{\text{D}} \ll \Gamma_{\text{T}}$.— In the regime $\Gamma_{\text{D}} \ll \Gamma_{\text{T}}$, the steady-state population of the dark modes remains negligible compared to that of the bright mode (see sketch in Fig. 1(c)). Introducing a small but finite Γ_{D} effectively opens an additional decay pathway into the trapping state, so that the total trapping rate becomes $\Gamma_{\text{T}} + \Gamma_{\text{D}}$. In this limit, the absorption cross section σ_{abs} coincides with that of a single effective atom with effective dipole moment $\sqrt{N}\varphi$ and enhanced radiative decay rate $N\Gamma_0$, upon replacing Γ_{T} by $\Gamma_{\text{T}} + \Gamma_{\text{D}}$:

$$\frac{\sigma_{\text{abs}}}{\sigma} \Big|_{\Gamma_{\text{D}} \ll \Gamma_{\text{T}}} = \frac{N\Gamma_0}{N\Gamma_0 + \Gamma_{\text{D}} + \Gamma_{\text{T}}} \cdot \frac{\Gamma_{\text{D}} + \Gamma_{\text{T}}}{N\Gamma_0 + \Gamma_{\text{D}} + \Gamma_{\text{T}}}. \quad (28)$$

Hence, σ_{abs} is maximum with value $\sigma_{\text{abs}}^{\text{max}} = \sigma/4$ now for $N\Gamma_0 = \Gamma_{\text{D}} + \Gamma_{\text{T}}$.

Arbitrary values of Γ_{T} and Γ_{D} .— As we have seen, Γ_{D} increases the transfer of excitations into dark long-lived modes, but at the same time, it reduces the scattering cross-section and thus the probability that an atom is excited. Therefore, we expect a non-trivial maximum of σ_{abs} as a function of Γ_{D} . In the general case, the absorption cross-section reads:

$$\frac{\sigma_{\text{abs}}}{\sigma} = \frac{N\Gamma_0}{N\Gamma_0 + \Gamma_{\text{D}} + \Gamma_{\text{T}}} \cdot \frac{\Gamma_{\text{D}} + \Gamma_{\text{T}}}{N\Gamma_0 + \Gamma_{\text{D}} + \Gamma_{\text{T}} + \Gamma_{\text{D}}\Gamma_0/\Gamma_{\text{T}}}, \quad (29)$$

which in the previously discussed regimes $\Gamma_{\text{T}}/\Gamma_{\text{D}} \ll 1$ and $\Gamma_{\text{T}}/\Gamma_{\text{D}} \gg 1$, leads to Eq. (27) and Eq. (28), respectively. The absorption cross section Eq. (29) of a nanoring with $N = 10$ and $N = 50$ emitters is plotted in Figs. 2 (b) and (c), respectively, as a function of the dimensionless parameters $\Gamma'_{\text{T}} \equiv \Gamma_{\text{T}}/N\Gamma_0$ and $\Gamma'_{\text{D}} \equiv \Gamma_{\text{D}}/N\Gamma_0$.

We can see that as we increase the value of N , σ_{abs} tends to the simple expression

$$\lim_{N \rightarrow \infty} \frac{\sigma_{\text{abs}}}{\sigma} = \frac{N\Gamma_0}{N\Gamma_0 + \Gamma_{\text{T}} + \Gamma_{\text{D}}} \cdot \frac{\Gamma_{\text{T}} + \Gamma_{\text{D}}}{N\Gamma_0 + \Gamma_{\text{T}} + \Gamma_{\text{D}}}, \quad (30)$$

with an absolute maximum of $\sigma_{\text{abs}}^{\text{max}} = \sigma/4$ when $\Gamma_{\text{T}} + \Gamma_{\text{D}} = N\Gamma_0$. This can be easily seen when writing $\sigma_{\text{abs}}/\sigma$ in terms of the parameters Γ'_{T} and Γ'_{D} , and neglecting $\Gamma'_{\text{D}}/N\Gamma'_{\text{T}}$ for $N \gg 1$.

In the general case, given a fixed value of Γ_0 and Γ_{T} , the maximum absorption occurs at:

$$\Gamma_{\text{D}}^{\text{max}} = \Gamma_0 \sqrt{\frac{N(N-1)\Gamma_{\text{T}}}{\Gamma_{\text{T}} + \Gamma_0}} - \Gamma_{\text{T}}. \quad (31)$$

This value is plotted in Fig. (2) (dashed black line). Note that imposing the condition $\Gamma_{\text{D}}^{\text{max}} > 0$ in Eq. (31) yields a constraint on the system parameters for the existence of a nontrivial maximum. This requirement can be written as $\Gamma_{\text{T}}(\Gamma_{\text{T}} + \Gamma_0)/\Gamma_0^2 < N(N-1)$, or equivalently,

$$\Gamma_{\text{T}}/\Gamma_0 < N - 1. \quad (32)$$

Therefore, the dimensionless trapping rate $\Gamma_{\text{T}}/\Gamma_0$ has to be small enough compared to the number of atoms. In fact, for a single atom ($N = 1$) and as expected from Eq. (23), dephasing is always detrimental and the maximum absorption occurs always at $\Gamma_{\text{D}}^{\text{max}} = 0$, regardless of the value of Γ_{T} . In contrast, when multiple atoms are present ($N \geq 2$), dephasing starts to be beneficial for small enough trapping rates.

At this optimal value of $\Gamma_{\text{D}}^{\text{max}}$, the absorption cross-section is given by:

$$\frac{\sigma_{\text{abs}}^{\text{max}}}{\sigma} = \left(\sqrt{\frac{N-1}{N}} + \sqrt{\frac{\Gamma_0 + \Gamma_{\text{T}}}{\Gamma_{\text{T}}}} \right)^{-2}. \quad (33)$$

It is straightforward to show that this value is always smaller or equal than $\sigma/4$. Specifically, by imposing the above condition given by Eq. (32), we arrive at $\sigma_{\text{abs}}^{\text{max}}/\sigma \leq (1 + N/(N-1))^{-2}$ which is always bounded by $1/4$. This result can be qualitatively understood as it follows. After an excitation is created, and regardless on how it is distributed among the collective eigenmodes, the system either emits a photon and returns back to the ground state with certain probability p , or it decays irreversibly into (t) with probability $1-p$. But the probability of absorbing the photon in the first place is always bounded by p (by time reversal symmetry), and therefore, the joint probability of absorption and subsequent conversion into (t) is at most $p(1-p)$, which has a maximum value of $1/4$ when $p = 1/2$.

V. COLLECTIVE ABSORPTION UNDER THERMAL DEPHASING

In the previous section, we demonstrated that dephasing redistributes population into dark modes, thus increasing the effective lifetime of the excitation and enhancing the absorption cross section. However, in that case the redistribution is at most uniform: in the steady state, all collective modes become equally populated. A natural question is whether the absorption can be further enhanced by selectively favoring the occupation of dark modes beyond this uniform limit.

Such selective population can indeed occur in the presence of thermal dephasing when the collective modes have

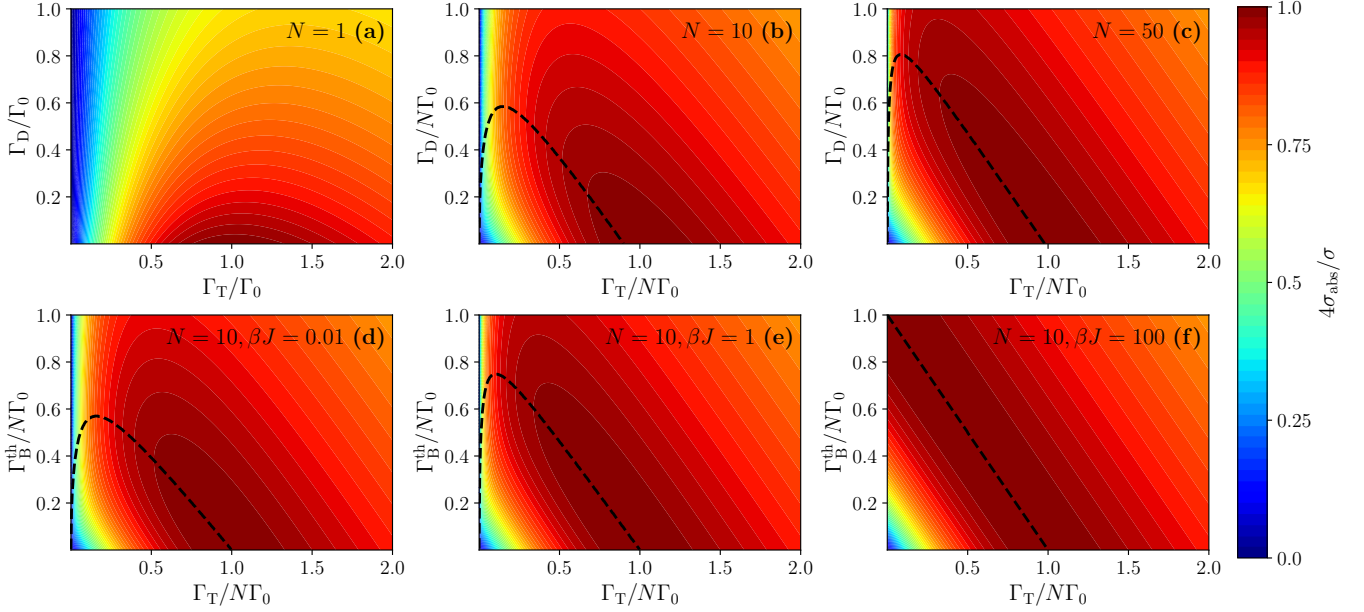


FIG. 2. Absorption cross-section σ_{abs} (in units of $\sigma/4$) in the presence of local (top panels) and thermal (bottom panels) dephasing, as a function of Γ_T and the dephasing rate (Γ_D or Γ_B^{th} , respectively), normalized to the bright mode spontaneous decay rate $N\Gamma_0$. (a) $N = 1$ (single emitter), where σ_{abs} decreases monotonically with Γ_D/Γ_0 and is maximal at $\Gamma_T = \Gamma_0$. (b) $N = 10$ and (c) $N = 50$. (d) $\beta J = 10^{-2}$, (e) $\beta J = 1$ and (f) $\beta J = 10^2$ for $N = 10$. All panels correspond to the Dicke (small-volume) limit. The dashed black line indicates the optimal dephasing rate maximizing σ_{abs} at fixed $\Gamma_T/N\Gamma_0$. σ_{abs} is always bounded by $\sigma/4$.

an appropriate energy dispersion, such as the one presented before (see Sec. II), with subradiant states lying at a lower energy. In this situation, a thermal environment tends to drive population toward these lower-energy weakly radiative states. As a result, thermal noise does not simply redistribute excitations uniformly, but can preferentially populate dark modes, potentially leading to a further enhancement of the absorption cross section. In the following, we analyze how is this effect depending on the temperature of the bath and the number of emitters.

The master equation Eq. (1) is now defined with $\mathcal{L} = \mathcal{L}_{\text{dd}} + \mathcal{L}_T + \mathcal{L}_{\text{th}}$. The reduced density matrix coefficients are now governed by Eq. (24a), together with:

$$\begin{aligned} \dot{\rho}_{gB} = & [-i(\tilde{J}_B - \delta) - (N\Gamma_0 + \Gamma_T + \sum_m k_{B \rightarrow m})/2] \rho_{gB} \\ & + i\sqrt{N}\Omega^*(\rho_{BB} - \rho_{gg}), \end{aligned} \quad (34a)$$

$$\begin{aligned} \dot{\rho}_{BB} = & -(N\Gamma_0 + \sum_m k_{B \rightarrow m} + \Gamma_T) \rho_{BB} + \sum_m k_{m \rightarrow B} \rho_{mm} \\ & + i\sqrt{N}(\Omega \rho_{gB} - \Omega^* \rho_{Bg}), \end{aligned} \quad (34b)$$

$$\dot{\rho}_{DD} = - \left(\sum_m k_{D \rightarrow m} + \Gamma_T \right) \rho_{DD} + \sum_m k_{m \rightarrow D} \rho_{mm}. \quad (34c)$$

As before, the index m in the summation runs over all possible states: the bright (B) and the dark modes ($D = \{1, \dots, N-1\}$).

Similarly as in Sec. IV we find for a weak driving field which is resonant with the bright mode that the steady state populations fulfill:

$$\Gamma_B^{\text{tot}} \rho_{BB} - \sum_m k_{m \rightarrow B} \rho_{mm} = \frac{4N|\Omega|^2}{\Gamma_B^{\text{tot}}}, \quad (35a)$$

$$\Gamma_D^{\text{tot}} \rho_{DD} - \sum_m k_{m \rightarrow D} \rho_{mm} = 0, \quad (35b)$$

where the total decay rate of a given mode m is given by $\Gamma_m^{\text{tot}} = \tilde{\Gamma}_m + \Gamma_T + \Gamma_m^{\text{th}}$, with $\Gamma_m^{\text{th}} \equiv \sum_{m'} k_{m \rightarrow m'}$.

For an arbitrary value of β , we can numerically solve this system of linear coupled equations to find the total excited state population $\rho_{ee} = \sum_{m=B,D} \rho_{mm}$. We then compute the absorption cross section from Eq. (12) and plot the results in Fig. 2(d)–(f) as a function of the dimensionless parameters $\Gamma_T/N\Gamma_0$ and $\Gamma_B^{\text{th}}/N\Gamma_0$, for different fixed values of βJ .

In this case, Γ_B^{th} takes the role of Γ_D in the pure local dephasing case (its explicit dependence on β and \tilde{f} can be found in Appendix B). Note also that for a fixed value of the inverse temperature β , Γ_B^{th} is proportional to the coupling strength \tilde{f} between the system and the phonon bath, so in each of the plots the vertical axis scale is proportional to this coupling.

Similarly to the case of pure local dephasing, we find that the absorption cross-section is again bounded by $\sigma/4$. This upper bound is not surprising as the same

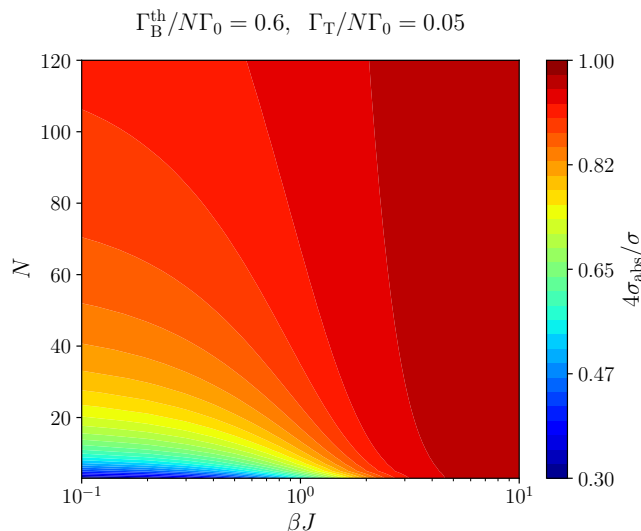


FIG. 3. Absorption cross section σ_{abs} (in units of $\sigma/4$) in presence of thermal dephasing and in the Dicke (small-volume) limit, at fixed values of $\Gamma_{\text{T}}/N\Gamma_0 = 0.6$ and $\Gamma_{\text{B}}^{\text{th}}/N\Gamma_0 = 0.05$, plotted versus N and βJ .

argument applies here as before: the probability that the photon is eventually absorbed is always bounded by $p(1-p) \leq 1/4$ ($0 \leq p \leq 1$).

In contrast to the pure local dephasing case, however, the maximum absorption is now attained when $\Gamma_{\text{T}} + \Gamma_{\text{B}}^{\text{th}} \approx N\Gamma_0$. Moreover, the region of parameter space where the absorption remains close to its maximal value expands towards smaller values of $\Gamma_{\text{T}}/N\Gamma_0$ as β increases (temperature decreases). In this sense, increasing β plays a role analogous to increasing the number of emitters N in the pure local dephasing case.

Thus, coupling the system to a low-temperature phonon bath enables the same absorption as in the pure local dephasing scenario, but with a smaller number of emitters. This is illustrated in Fig. 3, where for a particular point in parameter space ($\Gamma_{\text{T}}/N\Gamma_0 = 0.05$, $\Gamma_{\text{B}}^{\text{th}}/N\Gamma_0 = 0.6$), we evaluate σ_{abs} as a function of the number of emitters N and the inverse temperature β . The results show that, along a contour line of constant σ_{abs} , the required number of emitters decreases as β increases.

Collective absorption enhancement compared to independent atoms.— The collective enhancement of light absorption in the presence of thermal dephasing can be quantified by comparing σ_{abs} to the total absorption cross-section of N independent emitters. As a reference, we use the single-emitter absorption cross-section with spontaneous emission rate Γ_0 and irreversible decay Γ_{T} , denoted by $\sigma_{\text{abs}}^{\text{1at}}(\Gamma_0)$ and given in Eq. (23). In Fig. 4, we plot the ratio $\sigma_{\text{abs}}/N\sigma_{\text{abs}}^{\text{1at}}(\Gamma_0)$ for both decoherence models. In the case of pure local dephasing, the independent emitters are assumed to have the same dephasing rate Γ_{D} as in the collective system. For thermal

dephasing, we set $\Gamma_{\text{D}} = \Gamma_{\text{B}}^{\text{th}}$ in Eq. (23), ensuring that independent emitters experience the same effective environmental coupling as in the collective case.

For the pure local dephasing case [Fig. (4) (a)], at fixed value of $\Gamma_{\text{T}}/N\Gamma_0$, the ratio always increases with increasing $\Gamma_{\text{D}}/N\Gamma_0$. In the limit of $\Gamma_{\text{D}}/N\Gamma_0 \rightarrow \infty$ the ratio reaches one, indicating that the nanoring performs equivalently to N independent emitters in transferring population to the target state. Physically, strong dephasing suppresses coherent correlations between emitters and collective interference, such that the absorption efficiency approaches the independent-emitter limit.

In stark contrast, in presence of thermal dephasing [Fig. (4) (b)], the ratio $\sigma_{\text{abs}}/N\sigma_{\text{abs}}^{\text{1at}}(\Gamma_0)$ can surpass one in the regime $\Gamma_{\text{T}} \ll \Gamma_{\text{B}}^{\text{th}}$. In Fig. 5 we plot the same ratio versus emitter number N for a particular value of $\beta J = 3$. We observe that as N increases this ratio saturates to a constant value, which increases with inverse temperature βJ , as shown in the inset of the same figure. Moreover, as we show in the following, for $\beta J \rightarrow \infty$, this ratio scales as $\sigma_{\text{abs}}/N\sigma_{\text{abs}}^{\text{1at}}(\Gamma_0) \sim \Gamma_0/\Gamma_{\text{T}}$, and thus, it arbitrarily increases when decreasing the trapping rate.

Zero temperature limit.— In the zero temperature limit ($\beta J \rightarrow \infty$) a transition between states with increasing energy is always forbidden, as the rates $k_{a \rightarrow b}$ vanish for $\omega_{ab} \leq 0$. Therefore, Eq. (35a) for the bright state population, which is higher in energy, decouples from the other set of equations (since $k_{D \rightarrow B} = 0$, for any dark state $D = \{1, \dots, N-1\}$), leading to:

$$\rho_{\text{BB}} = \frac{4N |\Omega|^2}{(\Gamma_{\text{B}}^{\text{tot}})^2} = \frac{4N |\Omega|^2}{(N\Gamma_0 + \Gamma_{\text{T}} + \Gamma_{\text{B}}^{\text{th}})^2}. \quad (36)$$

The population of the remaining $N-1$ dark modes can be found iteratively solving the $N-1$ equations Eq. (35b) in descending order in energy. Moreover, summing Eq. (35b) over all possible dark modes, we obtain the balance equation $\Gamma_{\text{T}} \sum_D \rho_{DD} - \Gamma_{\text{B}}^{\text{th}} \rho_{\text{BB}} = 0$, which directly leads to

$$\rho_{ee} = \frac{\Gamma_{\text{B}}^{\text{th}} + \Gamma_{\text{T}}}{\Gamma_{\text{T}}} \rho_{\text{BB}}. \quad (37)$$

Using Eq. (37) together with Eq. (36) in Eq. (12) we find the simple expression for the absorption cross-section:

$$\left. \frac{\sigma_{\text{abs}}}{\sigma} \right|_{\beta J \rightarrow \infty} = \frac{N\Gamma_0}{N\Gamma_0 + \Gamma_{\text{T}} + \Gamma_{\text{B}}^{\text{th}}} \cdot \frac{\Gamma_{\text{T}} + \Gamma_{\text{B}}^{\text{th}}}{N\Gamma_0 + \Gamma_{\text{T}} + \Gamma_{\text{B}}^{\text{th}}}, \quad (38)$$

in agreement with Fig. (2)(f). Interestingly, this expression closely resembles the result obtained for the local dephasing model Eq. (30) in the limit $N \rightarrow \infty$, after replacing Γ_{D} by $\Gamma_{\text{B}}^{\text{th}}$.

From Eq. (38) one can further obtain an analytical expression for the ratio between the collective absorption cross-section and the one corresponding to N independent emitters. In the regime $\Gamma_{\text{T}} \ll \Gamma_0, \Gamma_{\text{B}}^{\text{th}}$ this ratio

tends to:

$$\begin{aligned} \lim_{N \rightarrow \infty} \frac{\sigma_{\text{abs}}}{N\sigma_{\text{abs}}^{\text{lat}}(\Gamma_0)} \Big|_{\beta J \rightarrow \infty} &= \frac{\Gamma_0(\Gamma_{\text{B}}^{\text{th}})^2}{\Gamma_{\text{T}}(N\Gamma_0 + \Gamma_{\text{B}}^{\text{th}})^2} \\ &= \frac{\Gamma_0}{\Gamma_{\text{T}}} \cdot \left(\frac{2\bar{f}J}{\Gamma_0 + 2\bar{f}J} \right)^2, \quad (39) \end{aligned}$$

where in the last equation we have used that $\Gamma_{\text{B}}^{\text{th}} = 2\bar{f}JN$ (see Eq. (C9) in Appendix C), i.e., that the thermal dephasing rate scales extensively with the number of emitters. As a consequence, in the presence of thermal dephasing the collective absorption cross section can exceed that of N independent emitters by an arbitrarily large factor as the ratio $\Gamma_{\text{T}}/\Gamma_0$ is reduced, as shown in Fig. (5).

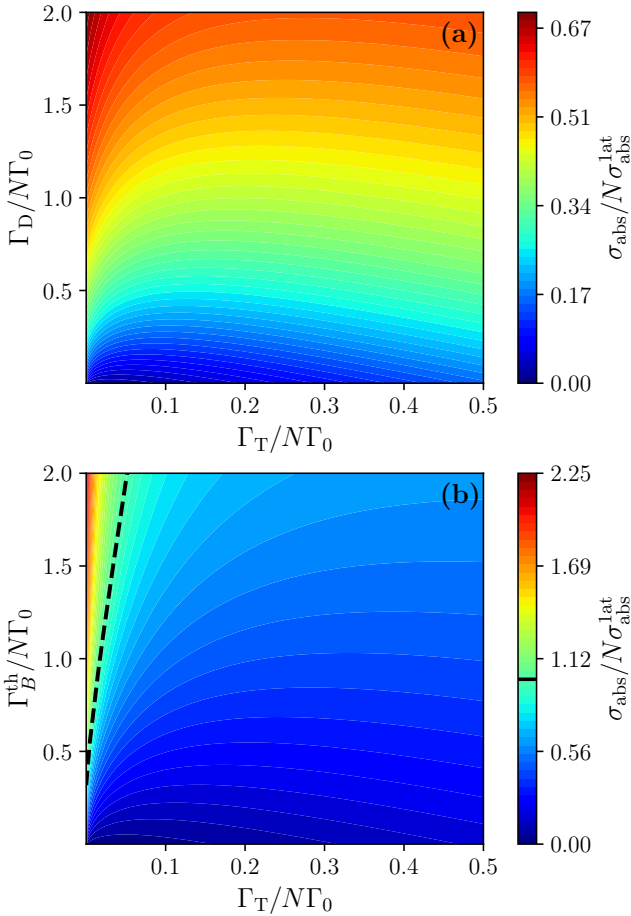


FIG. 4. Ratio of the collective absorption cross-section σ_{abs} of a nanoring to that of N independent emitters as a function of trapping ($\Gamma_{\text{T}}/N\Gamma_0$) and dephasing ($\Gamma_{\text{D}}/N\Gamma_0$ and $\Gamma_{\text{B}}^{\text{th}}/N\Gamma_0$) rates. (a) Pure local dephasing and (b) thermal dephasing with $\beta J = 1$. In the independent emitter case, each emitter has spontaneous emission rate Γ_0 , trapping rate Γ_{T} , and the dephasing rate is taken to be Γ_{D} or $\Gamma_{\text{B}}^{\text{th}}$, respectively. The dashed line marks 1, corresponding to equal absorption in the collective and independent cases. Results are shown for $N = 10$ in the Dicke (small-volume) limit.

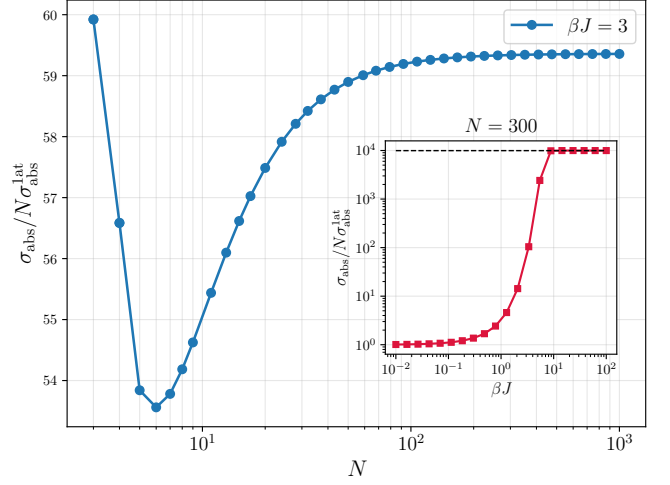


FIG. 5. Scaling of the ratio $\sigma_{\text{abs}}/N\sigma_{\text{abs}}^{\text{lat}}$ with the number of emitters N , in the presence of thermal dephasing, for $\beta J = 3$. For sufficiently large arrays ($N \gtrsim 100$), the ratio approaches a saturation value that depends on βJ . Inset: Saturation value of $\sigma_{\text{abs}}/N\sigma_{\text{abs}}^{\text{lat}}(\Gamma_0)$, extracted for $N = 300$, as a function of βJ . The gray dashed line marks the asymptotic low temperature limit from Eq. (39), scaling as $\sim \Gamma_0/\Gamma_{\text{T}}$. The trapping rate and coupling strength to the bath are fixed to $\Gamma_{\text{T}}/\Gamma_0 = 10^{-4}$ and $\bar{f} = 10^{-7}$, respectively.

VI. FINITE-SIZE EFFECTS IN RING GEOMETRIES

Up to now we have considered the idealized case where all emitters are contained in a very small volume ($d \ll \lambda_0$), therefore coupling homogeneously to the electromagnetic field. In this regime, commonly referred to as the Dicke limit, there exists only a single bright mode with enhanced decay rate $N\Gamma_0$, and $N - 1$ perfectly dark modes with vanishing decay rate.

We now move beyond this limit and consider a ring of finite spatial extent. In free space, the coupling to the electromagnetic field is no longer homogeneous, and the dark modes acquire a small finite decay rate.

In the limit of large interparticle separation d/λ_0 , the emitters behave independently and the absorption cross section approaches that of N uncorrelated emitters, namely, $\sigma_{\text{abs}} = N\sigma_{\text{abs}}^{\text{lat}}(\Gamma_0)$. However, for intermediate values of d/λ_0 , the behavior of σ_{abs} is nontrivial. On the one hand, the finite decay rate of subradiant modes reduces the excited-state population and thus σ_{abs} . On the other hand, these modes acquire a finite overlap with the driving field, which can increase their population and enhance ρ_{ee} and σ_{abs} . The competition between these two effects determines the absorption efficiency in the finite-size regime.

To assess the persistence of the enhancement mechanism discussed above, we analyze the dependence of σ_{abs} on the ratio d/λ_0 . The system dynamics are governed by equations analogous to Eq. (35a), but now each collective

mode m is driven with amplitude $\Omega_m = \sum_i \langle m|i\rangle \Omega(\mathbf{r}_i)$. In the steady state the mode populations fulfill (see Appendix E for details):

$$\Gamma_m^{\text{tot}} \rho_{mm} - \sum_{m'} k_{m' \rightarrow m} \rho_{m'm'} = \frac{4|\Omega_m|^2 \Gamma_m^{\text{tot}}}{(\Gamma_m^{\text{tot}})^2 + 4(\bar{J}_m - \delta)^2}. \quad (40)$$

For concreteness, we consider a plane-wave drive propagating along the \hat{x} direction with transverse linear polarization, $\Omega(\mathbf{r}_i) = \Omega_0 e^{ik_0 x_i}$. The detuning is chosen to match the frequency shift of the mode that couples most strongly to light, i.e., the brightest mode with maximal decay rate Γ_B . The value of Γ_B exhibits oscillations as a function of d/λ_0 , reflecting interference of the scattered fields (see Fig. 9 in Appendix D).

Solving Eq. (40) yields the total excited-state population $\rho_{ee} = \sum_m \rho_{mm}$ and, from Eq. (12), the absorption cross section. In Fig. 6, we plot σ_{abs} for $N = 10$ emitters as a function of Γ_T and Γ_B^{th} , normalized by the decay rate of the brightest mode Γ_B . The top panels correspond to $\beta\Gamma_0 = 0.01$ (local pure dephasing regime), while the bottom panels correspond to $\beta\Gamma_0 = 10$ (low-temperature thermal dephasing). Each panel represents a different value of the interparticle spacing, as indicated.

The results show that the enhancement of absorption with increasing Γ_B^{th} at low Γ_T persists beyond the Dicke limit. As in the fully collective regime, thermal dephasing enlarges the region of parameter space where absorption is maximized, and this effect becomes more pronounced at lower temperatures. However, for $d/\lambda_0 \gtrsim 0.3$, the enhancement due to thermal dephasing vanishes, and the optimal absorption is obtained for $\Gamma_B^{\text{th}} \approx 0$.

We also observe, as can be seen in Fig. 7, that the absolute maximum of σ_{abs} in parameter space increases with d/λ_0 before eventually approaching the independent-emitter limit. By optimizing σ_{abs} over Γ_T and Γ_B^{th} for each spacing, we obtain the maximal achievable absorption as a function of d/λ_0 . This quantity exhibits an oscillatory dependence reflecting interference effects, and asymptotically converges to the expected independent-emitter maximum value, $N\sigma/4$.

VII. ABSORPTION UNDER INCOHERENT ILLUMINATION

Up to now we have considered coherent driving. We now turn to a different scenario in which the system is illuminated by a field that is spatially coherent but temporally incoherent, such as broadband or thermal radiation (e.g. mimicking sunlight), modeled as a photonic bath following a thermal distribution.

Accordingly, we set $\Omega = 0$ and include the additional Lindblad contribution

$$\mathcal{L}_{\text{inc}}[\rho] = \epsilon N \Gamma_0 \left[(n+1) S \rho S^\dagger + n S^\dagger \rho S - \frac{1}{2} \left\{ (n+1) S^\dagger S + n S S^\dagger, \rho \right\} \right], \quad (41)$$

where $S^\dagger = N^{-1/2} \sum_i \hat{\sigma}_i^{eg}$ creates an excitation in the fully symmetric (bright) mode. The parameter $\epsilon \ll 1$ characterizes the light intensity, while n denotes the mean photon number of the incident field, for instance following a Bose–Einstein distribution at the photon temperature.

The incident photon rate is therefore $\dot{n}_{\text{in}} = \epsilon n N \Gamma_0$. Analogously to the coherent case, we define the absorption cross section through $\sigma_{\text{abs}}/A = \dot{n}_{\text{abs}}/\dot{n}_{\text{in}}$, yielding

$$\frac{\sigma_{\text{abs}}^{\text{inc}}}{\sigma} = \frac{\Gamma_T}{\epsilon n N \Gamma_0} \rho_{ee}. \quad (42)$$

The reduced density matrix elements now obey

$$\dot{\rho}_{gg} = \epsilon N \Gamma_0 [(n+1)\rho_{BB} - n\rho_{gg}] + N \Gamma_0 \rho_{BB}, \quad (43a)$$

$$\begin{aligned} \dot{\rho}_{BB} = \epsilon N \Gamma_0 [n\rho_{gg} - (n+1)\rho_{BB}] - \Gamma_B^{\text{tot}} \rho_{BB} \\ + \sum_m k_{m \rightarrow B} \rho_{mm}, \end{aligned} \quad (43b)$$

while the dark mode populations ρ_{DD} ($D = \{1, \dots, N-1\}$) evolve as in Eq. (35b).

In the weak-intensity limit ($\epsilon \ll 1$), we approximate $\rho_{gg} = 1 - \mathcal{O}(\epsilon^2)$. Under this condition, the steady-state populations satisfy the same algebraic equations as in the coherently driven case, Eq. (35a) and Eq. (35b), upon replacing $4N|\Omega|^2/\Gamma_B^{\text{tot}} \rightarrow \epsilon N \Gamma_0 n$.

The algebraic equations above can be solved numerically for arbitrary values of βJ . As in the coherent case, however, the limits $\beta J \rightarrow 0$ (corresponding to pure local dephasing) and $\beta J \rightarrow \infty$ (zero-temperature thermal dephasing) admit simple analytical expressions.

In the high-temperature limit $\beta J \rightarrow 0$, we obtain:

$$\rho_{ee} = \frac{\epsilon N \Gamma_0 n (\Gamma_T + \Gamma_D)}{\Gamma_T (N \Gamma_0 + \Gamma_D + \Gamma_T) + \Gamma_D \Gamma_0}, \quad (44)$$

$$\frac{\sigma_{\text{abs}}}{\sigma} = \frac{\Gamma_T + \Gamma_D}{N \Gamma_0 + \Gamma_D + \Gamma_T + \Gamma_D \Gamma_0 / \Gamma_T}. \quad (45)$$

According to this expression, the absorption cross section increases monotonically with the dephasing rate Γ_D . This behavior can be understood as follows: under broadband illumination, dephasing does not suppress the excitation probability, while it continues to redistribute population from radiative to subradiant collective modes. As a result, Γ_D enhances the effective trapping efficiency without reducing the probability of photon absorption. This is not the case for a single quantum emitter under incoherent illumination. Consider, in particular, a single emitter that couples to light with the same strength as the bright collective mode, and therefore decays radiatively at rate $N \Gamma_0$. For such an emitter the absorption cross section is simply $\sigma_{\text{abs}}^{\text{lat,inc}}(N \Gamma_0) = \Gamma_T / (N \Gamma_0 + \Gamma_T)$.

We note that in the regime $\Gamma_D \gg N \Gamma_0, \Gamma_T$, where all collective modes are equally populated, $\sigma_{\text{abs}}^{\text{inc}}/\sigma = \Gamma_T / (\Gamma_0 + \Gamma_T)$, which means that the trapping rate required to reach a given absorption efficiency is reduced by a factor of N compared to the single emitter case with

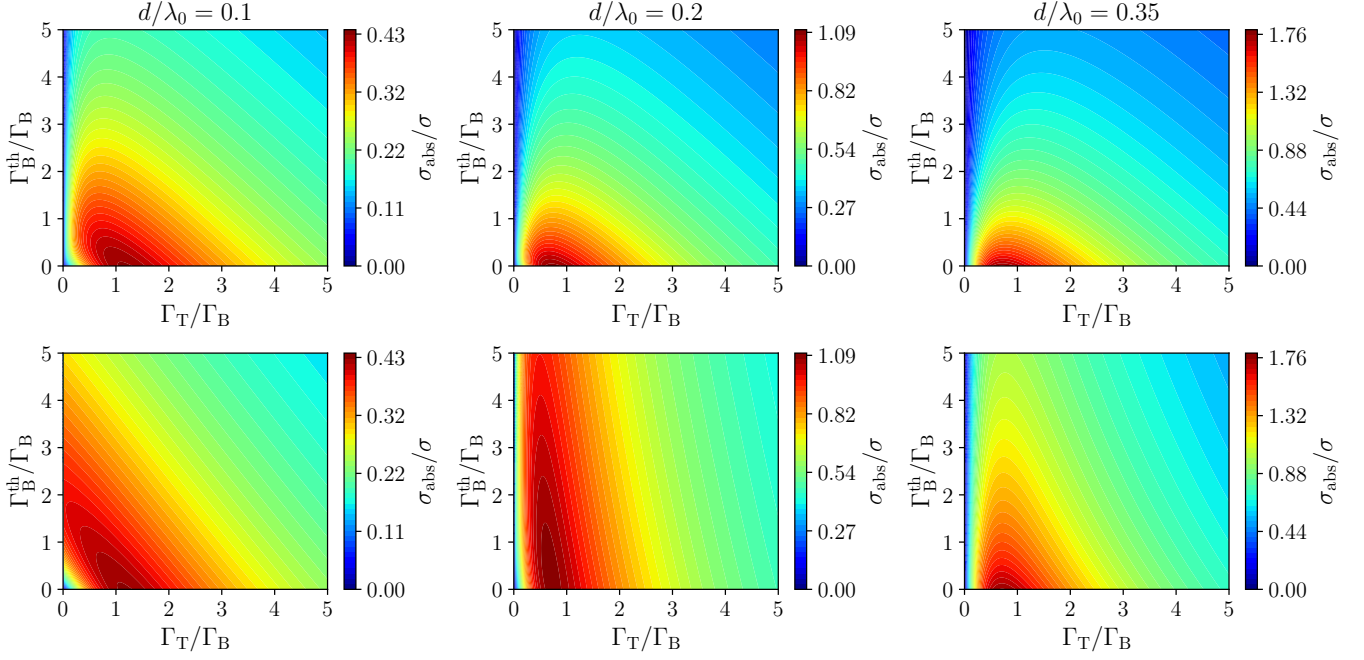


FIG. 6. Absorption cross-section σ_{abs} for a finite-size ring. σ_{abs} (in units of σ) is plotted versus trapping Γ_T and thermal dephasing Γ_B^{th} rates, normalized to the bright mode spontaneous decay rate Γ_B , for different values of $d/\lambda_0 = 0.1, 0.2, 0.35$. Top and bottom panels are for $\beta\Gamma_0 = 0.01$ (high temperature or local dephasing) and $\beta\Gamma_0 = 10$ (low temperature), respectively. The number of emitters is $N = 10$.

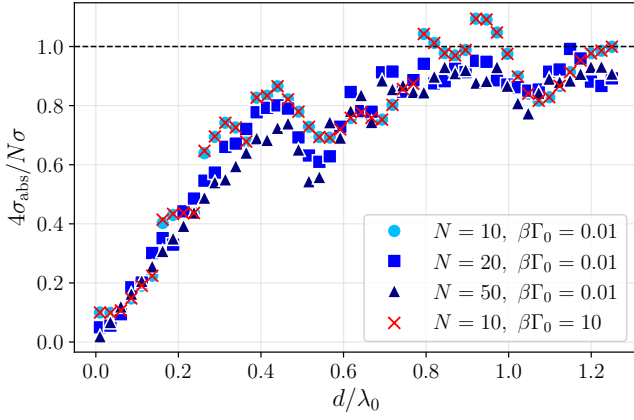


FIG. 7. Maximum absorption cross-section $4\sigma_{\text{abs}}/N\sigma$ (optimized over Γ_T and Γ_B^{th}) for a finite-size ring, as a function of d/λ_0 at fixed value of $\beta\Gamma_0$. $N = 10, \beta\Gamma_0 = 0.01$ (light blue circles); $N = 20, \beta\Gamma_0 = 0.01$ (blue squares); $N = 50, \beta\Gamma_0 = 0.01$ (dark blue triangles). Results for $N = 10, \beta\Gamma_0 = 10$ (red crosses) show negligible deviation from the $\beta\Gamma_0 = 0.01$ case with the same number of emitters. The dashed black line indicates the maximum absorption cross-section for N independent emitters.

decay $N\Gamma_0$. By contrast, in the opposite limit $\Gamma_D \ll \Gamma_T$, $\sigma_{\text{abs}}^{\text{inc}}/\sigma = (\Gamma_T + \Gamma_D)/(N\Gamma_0 + \Gamma_T + \Gamma_D)$ the absorption reduces to that of the single emitter with enhanced irreversible decay rate $\Gamma_T + \Gamma_D$.

Interestingly, the same expression for the absorption cross section is recovered by averaging the coherent scattering cross section under coherent illumination over all possible detunings (see Appendix F), highlighting the equivalence between broadband driving and frequency-averaged coherent excitation.

Now we move to the opposite low-temperature limit $\beta J \rightarrow \infty$, in which

$$\rho_{ee} = \frac{\epsilon N \Gamma_0 n (\Gamma_T + \Gamma_B^{\text{th}})}{\Gamma_T (N \Gamma_0 + \Gamma_T + \Gamma_B^{\text{th}})}, \quad (46)$$

$$\frac{\sigma_{\text{abs}}}{\sigma} = \frac{\Gamma_T + \Gamma_B^{\text{th}}}{N \Gamma_0 + \Gamma_T + \Gamma_B^{\text{th}}}. \quad (47)$$

Again, the absorption cross section increases monotonically with the thermal dephasing rate Γ_B^{th} . In this limit, σ_{abs} coincides with that of a single effective emitter characterized by an enhanced trapping rate $\Gamma_T + \Gamma_B^{\text{th}}$ and a collective radiative decay rate $N\Gamma_0$.

Figure 8 shows the absorption cross-section behavior versus $\Gamma_T/N\Gamma_0$ and $\Gamma_D/N\Gamma_0$ (or $\Gamma_B^{\text{th}}/\Gamma_0$) in the two limiting regimes $\beta J \rightarrow 0$ and $\beta J \rightarrow \infty$. More generally, we observe that environmental dephasing provides a mechanism to achieve the same absorption efficiency at lower trapping rates Γ_T , regardless of the photon bath temperature.

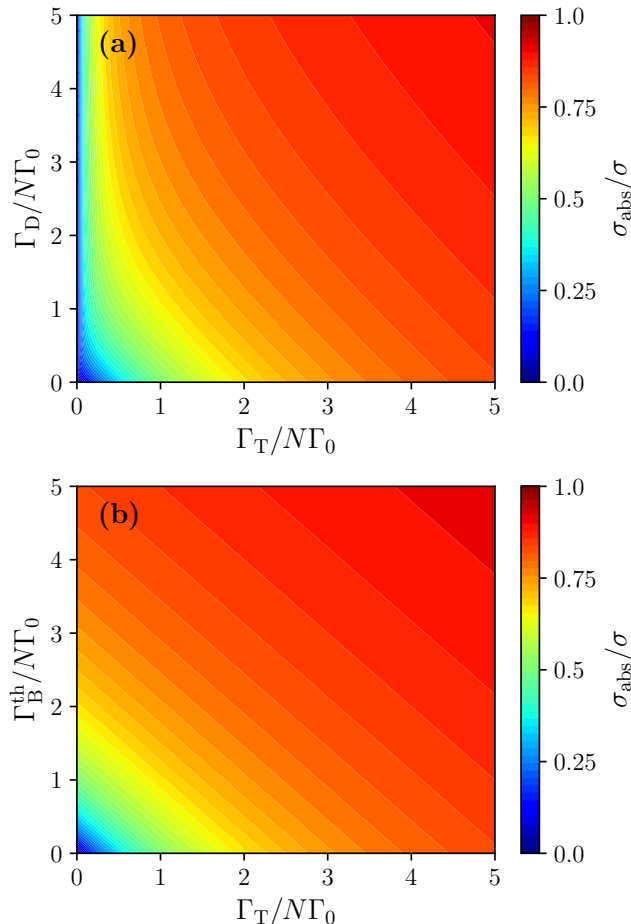


FIG. 8. Absorption cross-section σ_{abs} (in units of σ) of a nano-ring of quantum emitters under incoherent light, versus trapping decay Γ_T and dephasing Γ_D or Γ_B^{th} rates, normalized to the bright mode spontaneous decay rate $N\Gamma_0$. **(a)** Local dephasing ($\beta J = 0$). **(b)** Low-temperature thermal dephasing ($\beta J \rightarrow \infty$). All plots are in the Dicke (small volume) limit.

VIII. CONCLUSIONS

We have shown that collective radiance and environmental dephasing can cooperate to enhance the single-photon absorption cross section in subwavelength nanorings of quantum emitters. Dephasing, typically viewed as detrimental, plays a constructive role here by redistributing population among collective eigenmodes. Depending on the bath temperature, it can populate long-lived subradiant states and thereby increase the effective excitation lifetime. Although the absorption cross-section

remains bounded, dephasing enables this bound to be reached for substantially smaller irreversible decay rates into the target state.

For pure local dephasing, increasing the number of emitters enhances absorption by increasing the number of dark modes into which population can be redistributed. For a fixed system size, thermal dephasing produces a similar effect upon lowering the bath temperature, which selectively drives population toward subradiant modes. As a result, thermal dephasing allows the collective absorption to surpass that of N independent emitters, in contrast to the pure local dephasing case.

We further have verified that the main enhancement mechanism survives beyond the Dicke limit: for finite-size rings it persists for interparticle spacings up to $d/\lambda_0 \lesssim 0.3$, where dephasing continues to enhance absorption at low Γ_T/Γ_0 . Moreover, under incoherent illumination, dephasing does not reduce the excitation probability and acts only through population redistribution. Consequently, the absorption increases monotonically with both Γ_D and Γ_B^{th} .

Together, these results highlight how collective dissipation and environmental noise can be harnessed as resources to optimize light absorption in engineered quantum optical structures. Moreover, we anticipate that similar population-redistribution mechanisms could be used to enhance excitation transport.

ACKNOWLEDGEMENTS

We are deeply grateful to D. E. Chang for proposing the original problem and for generously sharing key early insights and guidance that were crucial in shaping the direction of this work. M.M.-C thanks C. Genes and A. Pal for insightful discussions. E.S.-L thanks Héctor Briongos-Merino and Guillem Lancis Beneyto for helpful discussions. We acknowledge funding from Grant PID2023-147475NB-I00 funded by MICIU/AEI/10.13039/501100011033 and by FEDER, UE. E.S.-L. acknowledges support from the 2025 FI STEP 00056 predoctoral grant of the Departament de Recerca i Universitats of the Generalitat de Catalunya, managed by AGAUR (10.13039/501100003030) and cofinanced by the European Social Fund Plus (ESF+), as well as from the Quantum Spain project funded by MICIU/AEI/10.13039/501100011033 and NextGenerationEU/PRTR. H. R. acknowledges support from the Austrian Science Fund (FWF) projects 10.55776/FG5 and the quantA cluster of excellence 10.55776/COE1.

-
- [1] R. J. Bettles, S. A. Gardiner, and C. S. Adams, *Physical Review Letters* **116**, 103602 (2016).
 [2] D. E. Chang, J. S. Douglas, A. González-Tudela, C.-L. Hung, and H. J. Kimble, *Reviews of Modern Physics* **90**,

- 031002 (2018).
 [3] J. Rui, D. Wei, A. Rubio-Abadal, S. Hollerith, J. Zeiher, D. M. Stamper-Kurn, C. Gross, and I. Bloch, *Nature* **583**, 369 (2020).

- [4] A. S. Sheremet, M. I. Petrov, I. V. Iorsh, A. V. Poshakinskiy, and A. N. Poddubny, *Reviews of Modern Physics* **95**, 015002 (2023).
- [5] A. Douglas, L. Su, M. Szurek, R. Groth, S. Brandstetter, O. Marković, O. Rubies-Bigorda, S. Ostermann, S. F. Yelin, and M. Greiner, “Many-body super- and subradiance in ordered atomic arrays,” (2026), arXiv:2604.11795 [quant-ph].
- [6] R. H. Dicke, *Physical Review* **93**, 99 (1954).
- [7] R. H. Lehmberg, *Physical Review A* **2**, 883 (1970).
- [8] M. Gross and S. Haroche, *Physics Reports* **93**, 301 (1982).
- [9] R. J. Bettles, S. A. Gardiner, and C. S. Adams, *Physical Review A* **92**, 063822 (2015).
- [10] A. Asenjo-Garcia, J. D. Hood, D. E. Chang, and H. J. Kimble, *Physical Review A* **95**, 033818 (2017).
- [11] A. Asenjo-Garcia, M. Moreno-Cardoner, A. Albrecht, H. J. Kimble, and D. E. Chang, *Physical Review X* **7**, 031024 (2017).
- [12] E. Shahmoon, D. S. Wild, M. D. Lukin, and S. F. Yelin, *Physical Review Letters* **118**, 113601 (2017).
- [13] J. Ruostekoski, *Physical Review A* **108**, 030101 (2023).
- [14] R. J. Bettles, S. A. Gardiner, and C. S. Adams, *Physical Review A* **94**, 043844 (2016).
- [15] M. Moreno-Cardoner, D. Plankensteiner, L. Ostermann, D. E. Chang, and H. Ritsch, *Physical Review A* **100**, 023806 (2019).
- [16] G. Ferioli, A. Glicenstein, F. Robicheaux, R. T. Sutherland, A. Browaeys, and I. Ferrier-Barbut, *Physical Review Letters* **127**, 243602 (2021).
- [17] J. Jiménez-Jaimes, S. Nic Chormaic, and E. Brion, *Physical Review A* **112**, 053702 (2025).
- [18] G. Facchinetti, S. D. Jenkins, and J. Ruostekoski, *Physical Review Letters* **117**, 243601 (2016).
- [19] M. Cech, I. Lesanovsky, and B. Olmos, *Physical Review A* **108**, L051702 (2023).
- [20] V. Paulisch, H. J. Kimble, and A. González-Tudela, *New Journal of Physics* **18**, 043041 (2016).
- [21] R. Bekenstein, I. Pikovski, H. Pichler, E. Shahmoon, S. F. Yelin, and M. D. Lukin, *Nature Physics* **16**, 676 (2020).
- [22] M. Moreno-Cardoner, D. Goncalves, and D. E. Chang, *Physical Review Letters* **127**, 263602 (2021).
- [23] K. Srakaew, P. Weckesser, S. Hollerith, D. Wei, D. Adler, I. Bloch, and J. Zeiher, *Nature Physics* **19**, 714 (2023).
- [24] J. A. Needham, I. Lesanovsky, and B. Olmos, *New Journal of Physics* **21**, 073061 (2019).
- [25] A. Pal, R. Holzinger, M. Moreno-Cardoner, and H. Ritsch, *New Journal of Physics* **27**, 094101 (2025).
- [26] L. Henriët, J. S. Douglas, D. E. Chang, and A. Albrecht, *Physical Review A* **99**, 023802 (2019).
- [27] D. Zafra-Bono, O. Rubies-Bigorda, and S. F. Yelin, “Subradiant collective states for precision sensing via transmission spectra,” (2025), arXiv:2512.09050 [quant-ph].
- [28] J. Perczel, J. Borregaard, D. E. Chang, H. Pichler, S. F. Yelin, P. Zoller, and M. D. Lukin, *Physical Review Letters* **119**, 023603 (2017).
- [29] A. Zhang, L. Wang, X. Chen, V. V. Yakovlev, and L. Yuan, *Communications Physics* **2**, 157 (2019).
- [30] M. Endres, H. Bernien, A. Keesling, H. Levine, E. R. Anschuetz, A. Krajenbrink, C. Senko, V. Vuletic, M. Greiner, and M. D. Lukin, *Science* **354**, 1024 (2016).
- [31] D. Barredo, S. de Léséleuc, V. Lienhard, T. Lahaye, and A. Browaeys, *Science* **354**, 1021 (2016).
- [32] D. Barredo, V. Lienhard, S. de Léséleuc, T. Lahaye, and A. Browaeys, *Nature* **561**, 79 (2018).
- [33] G. Ferioli, A. Glicenstein, L. Henriët, I. Ferrier-Barbut, and A. Browaeys, *Physical Review X* **11**, 021031 (2021).
- [34] A. Tiranov, V. Angelopoulos, C. J. van Diepen, B. Schirnski, O. A. D. Sandberg, Y. Wang, L. Midolo, S. Scholz, A. D. Wieck, A. Ludwig, A. S. Sørensen, and P. Lodahl, *Science* **379**, 389 (2023).
- [35] A. F. van Loo, A. Fedorov, K. Lalumière, B. C. Sanders, A. Blais, and A. Wallraff, *Science* **342**, 1494 (2013).
- [36] R. Holzinger, D. Plankensteiner, L. Ostermann, and H. Ritsch, *Physical Review Letters* **124**, 253603 (2020).
- [37] S. Bourne Worster, C. Stross, F. M. W. C. Vaughan, N. Linden, and F. R. Manby, *The Journal of Physical Chemistry Letters* **10**, 7383 (2019).
- [38] D. Montemayor, E. Rivera, and S. J. Jang, *The Journal of Physical Chemistry B* **122**, 3815 (2018).
- [39] P. Reberntrost, M. Mohseni, I. Kassal, S. Lloyd, and A. Aspuru-Guzik, *New Journal of Physics* **11**, 033003 (2009).
- [40] F. Mattiotti, M. Sarovar, G. G. Giusteri, F. Borgonovi, and G. L. Celardo, *New Journal of Physics* **24**, 013027 (2022).
- [41] M. Moreno-Cardoner, R. Holzinger, and H. Ritsch, *Optics Express* **30**, 10779 (2022).
- [42] V. Scheil, R. Holzinger, M. Moreno-Cardoner, and H. Ritsch, *Nanomaterials* **13**, 851 (2023).
- [43] M. Eltoha and F. Robicheaux, *Physical Review A* **112**, 023112 (2025).
- [44] A. Mattioni, F. Caycedo-Soler, S. F. Huelga, and M. B. Plenio, **11**, 041003.
- [45] J. Adolphs and T. Renger, *Biophysical Journal* **91**, 2778 (2006).
- [46] T. Renger and R. A. Marcus, *The Journal of Chemical Physics* **116**, 9997 (2002).
- [47] A. Ishizaki and G. R. Fleming, *Proceedings of the National Academy of Sciences* **106**, 17255 (2009).
- [48] P. Reberntrost, M. Mohseni, and A. Aspuru-Guzik, *The Journal of Physical Chemistry B* **113**, 9942 (2009).
- [49] P. Nalbach, D. Braun, and M. Thorwart, *Physical Review E* **84**, 041926 (2011).
- [50] H.-B. Chen, N. Lambert, Y.-C. Cheng, Y.-N. Chen, and F. Nori, *Scientific Reports* **5**, 12753 (2015).
- [51] Formally, we should also include the evolution of the target (t) state population, $\dot{\rho}_{tt} = \Gamma_T \rho_{ee}$. However, imposing instead $\dot{\rho}_{gg} = \dot{\rho}_{tt} = 0$ would lead to the trivial solution that in steady state all atoms are in (t), as the trapping channel is the only irreversible channel under consideration. We are here instead looking for the asymptotic long-time value of ρ_{ee} before it finally decays into (t).
- [52] H.-P. Breuer, *The Theory of Open Quantum Systems* (Clarendon, Oxford, 2007).
- [53] F. Caruso, A. W. Chin, A. Datta, S. F. Huelga, and M. B. Plenio, *Physical Review A* **81**, 062346 (2010).

Appendix A: Microscopic origin of pure local and thermal dephasing models

The dephasing models considered in this work can naturally arise by coupling the system of emitters with a thermal phononic bath, which can be described by an ensemble of harmonic oscillators. In natural light-harvesting complexes, the phononic bath accounts for the vibrational motions of the surrounding molecular and protein environment, whereas in artificial light-harvesting complexes it typically represents the lattice vibrations of the substrate or host material that couples to the electronic excitations.

The starting point is the Hamiltonian in the single excitation subspace, which can be written as $\hat{H} = \sum_{\alpha} \omega_{\alpha} |\alpha\rangle\langle\alpha| + \sum_q \omega_q \hat{c}_q^{\dagger} \hat{c}_q + \hat{H}_{\text{SB}}$. The first term corresponds to the bare system Hamiltonian written in the diagonal collective basis $\{|\alpha\rangle\}$, whereas the second term refers to the energy of the vibrational degrees of freedom, described by the creation \hat{c}_q^{\dagger} and annihilation c_q operators of a bath excitation. In the so-called Born-Oppenheimer approximation, which applies when there exists a separation of the time scales in the evolution of the system and the bath, the system-phononic bath interaction takes the generic form [44]:

$$\hat{H}_{\text{SB}} = \sum_i |i\rangle\langle i| \left[\sum_q \xi_{qi} (\hat{c}_q + \hat{c}_q^{\dagger}) \right],$$

where ξ_{qi} is the coupling strength between emitter at position i and the normal bath mode q , and it depends on the microscopic details of the bath.

Following standard theory of open quantum systems [52, 53], and if we restrict to the single excitation subspace, the Born-Markov and rotating wave approximations lead to the following Lindblad master equation for the system evolution:

$$\dot{\rho} = \sum_{\omega, i, j} \Gamma_{ij}(\omega) \left[2A_j(\omega) \rho A_i^{\dagger}(\omega) - \left\{ A_i^{\dagger}(\omega) A_j(\omega), \rho \right\} \right],$$

with $A_i(\omega) = \sum_{\omega_{\beta} - \omega_{\alpha} = \omega} |\alpha\rangle\langle\alpha| i \langle i | \beta \rangle \langle \beta |$ and $|\alpha\rangle, |\beta\rangle$ denoting the collective eigenmodes of the system.

The couplings $\Gamma_{ij}(\omega)$ correspond to the Fourier transform of the bath correlation functions and are given by

$$\Gamma_{ij}(\omega) = \int_{-\infty}^{\infty} ds e^{i\omega s} \langle B_i^{\dagger}(s) B_j(0) \rangle,$$

with $B_i^{\dagger}(t) = \sum_q \xi_{qi} (e^{i\omega_q t} \hat{c}_q + e^{-i\omega_q t} \hat{c}_q^{\dagger})$. Following [44] we will then approximate that the spatial correlation part factorizes from this expression, such that we can write $\Gamma_{ij}(\omega) = \eta_{ij} \Gamma(\omega)$, and the value of η_{ij} describes the range of spatial correlations of the bath.

We restrict here to a phononic bath that is in thermal equilibrium, following a Bose-Einstein distribution at temperature T , $n(\omega) = (e^{\beta\omega} - 1)^{-1}$. After doing some algebra we arrive at the general expression

$$\Gamma_{ij}(\omega) = \eta_{ij} 2\pi [\mathcal{J}(\omega)(1 + n(\omega)) + \mathcal{J}(-\omega)n(-\omega)],$$

where $\mathcal{J}(\omega) = \sum_{q,i} \xi_{qi}^2 \delta(\omega - \omega_q)$ is the spectral density of the bath. Moreover, we will restrict ourselves to the case of local correlations, $\eta_{ij} = \delta_{ij}$, and define $\Gamma(\omega) = \Gamma_{ii}(\omega)$.

In the collective basis, we can then rewrite:

$$A_j(\omega) \rho A_j^{\dagger}(\omega) = \sum |\alpha\rangle\langle\alpha| j \langle j | \beta \rangle \langle \beta | \rho | \beta' \rangle \langle \beta' | j \rangle \langle j | \alpha' \rangle \langle \alpha' |, \quad (\text{A1})$$

where the summation runs over all states such that $\omega_{\beta} - \omega_{\alpha} = \omega$ and $\omega_{\beta'} - \omega_{\alpha'} = \omega$. According to this expression, the dynamics of the diagonal elements of the density matrix $\rho_{\alpha\alpha}$ will only have contributions from $\rho_{\beta\beta'}$ such that $\omega_{\beta} = \omega_{\beta'}$. Taking into account the form of the eigenstates Eq. (6), and that $\langle \alpha | j \rangle \langle j | \beta \rangle \langle \beta' | j \rangle \langle j | \alpha' \rangle \propto \delta_{\alpha - \beta + \beta' - \alpha'}$, together with the fact that the spectrum is anharmonic for the considered case, only the diagonal terms $\rho_{\beta\beta}$ will play a role in the population dynamics. In this situation, the population dynamics are then described by the equation:

$$\dot{\rho} = \sum_{\omega = \omega_{\beta} - \omega_{\alpha}} \Gamma(\omega) [2|\alpha\rangle\langle\beta| \rho |\beta\rangle\langle\alpha| - \{|\beta\rangle\langle\beta|, \rho\}], \quad (\text{A2})$$

which is equivalent to Eq. (15).

Appendix B: Bright mode thermal dephasing rate

The thermal decay rate of the bright mode is defined as:

$$\Gamma_{\text{B}}^{\text{th}} = \sum_m k_{\text{B} \rightarrow m}, \quad (\text{B1})$$

where $k_{\text{B} \rightarrow m}$, given by Eq. (18), is the transition rate from the bright mode to any other mode m . Considering the Ohmic limit in the spectral density function and the tight-binding dispersion relation Eq. (10) we obtain:

$$\frac{\Gamma_{\text{B}}^{\text{th}}}{2fJ} = \sum_m \frac{1 - \cos\left(\frac{2\pi m}{N}\right)}{1 - \exp\{-\beta J [1 - \cos\left(\frac{2\pi m}{N}\right)]\}}, \quad (\text{B2})$$

with $m \in [-N/2, N/2]$. Taking the continuum limit $N \rightarrow \infty$ and defining $x = 2\pi m/N$ we can write the previous result as the integral:

$$\frac{\Gamma_{\text{B}}^{\text{th}}}{2fJ} = \frac{N}{2\pi} \int_{-\pi}^{\pi} dx \frac{1 - \cos x}{1 - e^{-\beta J (1 - \cos x)}}. \quad (\text{B3})$$

As $|\cos x| \leq 1$ and $\beta J > 0$ the exponential in the denominator is always smaller than unity and the geometric series formula can be applied, leading to:

$$\frac{\Gamma_{\text{B}}^{\text{th}}}{2fJ} = \frac{N}{2\pi} \int_{-\pi}^{\pi} dx (1 - \cos x) \sum_{n=0}^{\infty} e^{-n\beta J (1 - \cos x)}. \quad (\text{B4})$$

Bringing the summation out of the integral we find:

$$\frac{\Gamma_{\text{B}}^{\text{th}}}{2fJ} = \frac{N}{2\pi} \sum_{n=0}^{\infty} e^{-\beta J n} \int_{-\pi}^{\pi} dx (1 - \cos x) e^{n\beta J \cos x}, \quad (\text{B5})$$

where the integral can be written in terms of the modified Bessel functions of First Kind $I_n(z)$. Thus,

$$\frac{\Gamma_B^{\text{th}}}{2N\bar{f}J} = \sum_{n=0}^{\infty} e^{-n\beta J} [I_0(n\beta J) - I_1(n\beta J)]. \quad (\text{B6})$$

This is a decreasing function with βJ . In the limit of zero temperature $\beta J \rightarrow \infty$ the summation on the right hand side is equal to 1, which means that $\Gamma_B^{\text{th}} = 2N\bar{f}J$. In the limit of $\beta J \rightarrow 0$ the summation scales as $(\beta J)^{-1}$.

Appendix C: Thermal dephasing rate in the zero temperature limit

Moreover, we can find an analytical expression for the thermal dephasing rate of an arbitrary collective mode m in the zero temperature limit. This is now defined as:

$$\Gamma_m^{\text{th}} = \sum_{m'} k_{m \rightarrow m'}, \quad (\text{C1})$$

with m' running over all other possible collective modes. In the zero-temperature limit $\beta J \rightarrow \infty$, only transitions to lower-energy modes are allowed. Using $k_{a \rightarrow b} = 2\bar{f} \text{ReLU}(\omega_{ab})$ and the convention $\omega_{mm'} = \tilde{J}_m - \tilde{J}_{m'}$, we obtain

$$\Gamma_m^{\text{th}} = \sum_{m'} 2\bar{f} \omega_{mm'} = 2\bar{f} \sum_{m'} (\tilde{J}_m - \tilde{J}_{m'}), \quad (\text{C2})$$

where the sum is restricted to modes m' such that $\tilde{J}_{m'} < \tilde{J}_m$.

We now make explicit this restriction using the dispersion relation. In the small-volume (Dicke) limit the collective shifts follow

$$\tilde{J}_m = J \cos\left(\frac{2\pi m}{N}\right), \quad J > 0. \quad (\text{C3})$$

Since $\tilde{J}_{-m} = \tilde{J}_m$, the energies depend only on $|m|$. Moreover, for $|m| \leq N/2$ the cosine decreases monotonically with $|m|$ away from $m = 0$, and therefore for any $|m| < N/2$,

$$\tilde{J}_{m'} < \tilde{J}_m \iff |m'| > |m|. \quad (\text{C4})$$

For the edge mode $m = \pm N/2$ in the even- N case there are no modes below it in energy.

With this identification, the restricted sum can be split into two contributions:

$$\Gamma_m^{\text{th}} = 2\bar{f} \left[\sum_{\tilde{J}_{m'} < \tilde{J}_m} \tilde{J}_m - \sum_{\tilde{J}_{m'} < \tilde{J}_m} \tilde{J}_{m'} \right]. \quad (\text{C5})$$

The first term is independent of m' and simply counts how many states satisfy $\tilde{J}_{m'} < \tilde{J}_m$, i.e. how many indices obey $|m'| > |m|$. This yields

$$\sum_{\tilde{J}_{m'} < \tilde{J}_m} \tilde{J}_m = \tilde{J}_m \max\{0, N - 2|m| - 1\}. \quad (\text{C6})$$

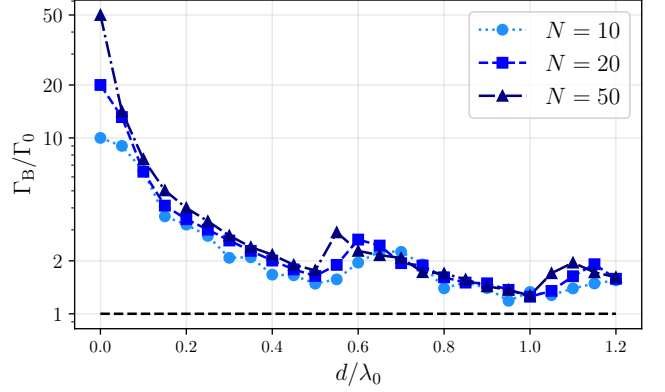


FIG. 9. Spontaneous decay rate of the bright mode, $\tilde{\Gamma}_B$, as a function of the interparticle distance d/λ_0 for $N = \{10, 20, 50\}$ emitters.

The max function accounts for the darkest states ($m = \pm N/2$ for even N or $m = \pm(N-1)/2$ for odd N), for which no lower-energy modes exist.

For the second term, we use again Eq. (C4) and evaluate

$$\sum_{\tilde{J}_{m'} < \tilde{J}_m} \tilde{J}_{m'} = \sum_{|m'| > |m|} J \cos\left(\frac{2\pi m'}{N}\right). \quad (\text{C7})$$

This restricted cosine sum admits a closed form, which can be written compactly as

$$\sum_{\tilde{J}_{m'} < \tilde{J}_m} \tilde{J}_{m'} = -J \max\left\{0, \csc\left(\frac{\pi}{N}\right) \sin\left(\frac{2\pi|m|}{N} + \frac{\pi}{N}\right)\right\}. \quad (\text{C8})$$

Again, the max function ensures the expression also holds for the darkest mode, for which the restricted sum vanishes.

Combining Eqs. Eq. (C3), Eq. (C6), and Eq. (C8), we obtain

$$\frac{\Gamma_m^{\text{th}}}{2\bar{f}J} = \cos\left(\frac{2\pi m}{N}\right) \max\{0, N - 2|m| - 1\} + \max\left\{0, \csc\left(\frac{\pi}{N}\right) \sin\left(\frac{2\pi|m|}{N} + \frac{\pi}{N}\right)\right\}. \quad (\text{C9})$$

As stated in the main text, the bright mode satisfies $\Gamma_B^{\text{th}} = 2\bar{f}JN$, while for the lowest-energy (darkest) modes the thermal decay vanishes, $\Gamma_m^{\text{th}} = 0$, since there are no states below them in energy.

Appendix D: Spontaneous decay right of the bright mode with a nanoring with finite size

In Fig. 9 we show how the spontaneous decay rate of the most radiant collective mode varies with the interparticle distance between the emitters in the nanoring. When $d \ll \lambda_0$ we enter in the deep subwavelength regime

or Dicke limit where $\tilde{\Gamma}_B \approx N\Gamma_0$ and the bright mode corresponds to the $|m=0\rangle$ state. As d increases $\tilde{\Gamma}_B$ shows an oscillatory behavior due to the changes in the interference pattern of the emitted field. In particular, the decay rate of the permutationally symmetric mode can be reduced, and for certain separations modes with $m \neq 0$ become more radiative than the symmetric one. As the separation between consecutive emitters goes beyond the subwavelength regime, the decay approaches the single atom spontaneous decay rate, $\tilde{\Gamma}_B \approx \Gamma_0$. This happens when we reach the independent emitters regime, where the effects of the dipole-dipole interactions become negligible.

Appendix E: Derivation of weak-driving equations for the finite-size ring

Here we generalize the single-mode weak-driving dynamical equations to the case where several collective modes are excited (finite-size ring), also in presence of a thermal dephasing bath. We work in the single-excitation

approximation with basis formed by the ground state $|g\rangle$ and the collective excited states $|m\rangle$. The density matrix evolves according to

$$\dot{\rho} = -i \left[(\hat{H}_{\text{eff}} + \hat{H}_{\text{in}})\rho - \rho(\hat{H}_{\text{eff}}^\dagger + \hat{H}_{\text{in}}) \right] + \sum_m \tilde{\Gamma}_m |g\rangle\langle m| \rho |m\rangle\langle g| + \mathcal{L}_{\text{th}}[\rho], \quad (\text{E1})$$

and in the collective basis the effective and input Hamiltonians can be written as:

$$\hat{H}_{\text{eff}} = \sum_m \left[-\delta_m - i\frac{\tilde{\Gamma}_m}{2} \right] |m\rangle\langle m|$$

$$\hat{H}_{\text{in}} = -\sum_m (\Omega_m |m\rangle\langle g| + \Omega_m^* |g\rangle\langle m|), \quad (\text{E2})$$

where $\Omega_m = \sum_i \langle m|i\rangle \Omega(\mathbf{r}_i)$ is the spatially dependent Rabi frequency projected onto collective mode m , and $\delta_m \equiv \delta - \tilde{J}_m$ is the detuning with respect to mode m .

From Eq. (E1), the ground-state population, ground-excited coherences and excited state density matrix elements obey, respectively:

$$\dot{\rho}_{gg} = \sum_m \tilde{\Gamma}_m \rho_{mm} + i \sum_m (\Omega_m^* \rho_{mg} - \Omega_m \rho_{gm}) \quad (\text{E3})$$

$$\dot{\rho}_{gm} = \left(i\delta_m - \frac{\Gamma_m^{\text{tot}}}{2} \right) \rho_{gm} + i \sum_n (\Omega_n^* \rho_{nm} - \Omega_m^* \rho_{gn}) \quad (\text{E4})$$

$$\dot{\rho}_{mm'} = \left[i(\delta_m - \delta_{m'}) - \frac{\tilde{\Gamma}_m + \tilde{\Gamma}_{m'}}{2} - \Gamma_T \right] \rho_{mm'} + i(\Omega_m \rho_{gm'} - \Omega_{m'}^* \rho_{mg}) + \delta_{mm'} \sum_b k_{b \rightarrow m} \rho_{bb} - \frac{1}{2} \sum_b (k_{m \rightarrow b} + k_{m' \rightarrow b}) \rho_{mm'}, \quad (\text{E5})$$

where we have defined the total decay rate (linewidth) of mode m as

$$\Gamma_m^{\text{tot}} \equiv \tilde{\Gamma}_m + \Gamma_T + \sum_b k_{m \rightarrow b}. \quad (\text{E6})$$

For the diagonal components, $m = m'$, this reduces to

$$\dot{\rho}_{mm} = -\Gamma_m^{\text{tot}} \rho_{mm} + \sum_b k_{b \rightarrow m} \rho_{bb} + i(\Omega_m \rho_{gm} - \Omega_m^* \rho_{mg}). \quad (\text{E7})$$

We now take the weak-driving limit. In this regime the system remains mostly in the ground state, $\rho_{gg} \simeq 1$, while the optical coherences are first order in the drive amplitude, $\rho_{gm}, \rho_{mg} = O(\Omega)$, and the excited-state populations and coherences are second order, $\rho_{mm'} = O(|\Omega|^2)$. Therefore, to leading order in the drive, the last term in Eq. (E4), which is proportional to $\Omega_n^* \rho_{nm}$, can be neglected. At steady state we obtain

$$0 = i\delta_m \rho_{gm} - \frac{\Gamma_m^{\text{tot}}}{2} \rho_{gm} + i\Omega_m^*. \quad (\text{E8})$$

Thus,

$$\rho_{gm}^{\text{st.}} = \frac{i\Omega_m^*}{i\delta_m - \Gamma_m^{\text{tot}}/2}, \quad (\text{E9})$$

and, equivalently,

$$\rho_{mg}^{\text{st.}} = \frac{i\Omega_m}{i\delta_m + \Gamma_m^{\text{tot}}/2}. \quad (\text{E10})$$

Substituting these weak-driving coherences into Eq. (E7), the optical source term becomes

$$i(\Omega_m \rho_{gm}^{\text{st.}} - \Omega_m^* \rho_{mg}^{\text{st.}}) = \frac{4|\Omega_m|^2 \Gamma_m^{\text{tot}}}{(\Gamma_m^{\text{tot}})^2 + 4(\tilde{J}_m - \delta)^2}. \quad (\text{E11})$$

Therefore, the steady-state population equation becomes

$$\Gamma_m^{\text{tot}} \rho_{mm} - \sum_{m'} k_{m' \rightarrow m} \rho_{m'm'} = \frac{4|\Omega_m|^2 \Gamma_m^{\text{tot}}}{(\Gamma_m^{\text{tot}})^2 + 4(\tilde{J}_m - \delta)^2}, \quad (\text{E12})$$

as in Eq. (40). This is a generalization of the single-mode weak-driving result. The left-hand side describes radiative loss plus thermal depletion of mode m , together with thermal feeding from the other collective modes. The right-hand side is the optical pumping rate into mode m , broadened by the total linewidth Γ_m^{tot} .

Appendix F: Broadband illumination (off-resonant light)

Here we show that incoherent (thermal) illumination yields the same steady-state populations as a coherently driven system after averaging over the detuning δ . Broadband excitation can be viewed as an ensemble of monochromatic drives with uniformly distributed frequencies, such that the incoherent result is recovered by integrating the coherent steady-state response over detuning, provided one identifies the effective incident photon flux via $4|\Omega|^2/N\Gamma_0 \rightarrow \epsilon n N\Gamma_0$.

Dephasing may be interpreted as rapid fluctuations of the transition frequency (equivalently, phase randomization). Under broadband illumination, the excitation probability is no longer sensitive to the detuning of a single monochromatic tone, because the response is effectively averaged over δ . As a result, the detuning-dependent reduction of the extinction is removed, and dephasing primarily affects the dynamics by redistributing population among available states rather than by suppressing coherent excitation.

The situation is particularly relevant in the collective case. For homogeneous local dephasing (i.e., identical dephasing rates on all sites), all collective modes experience the same statistical frequency fluctuations, and the population exchange between collective modes is not impeded by detuning. More generally, for inhomogeneous

dephasing one still obtains mode mixing whenever the corresponding overlap factors in the collective basis remain nonzero; however, the effective exchange rates typically decrease as the inhomogeneity increases.

To make the equivalence explicit, we consider the detuning-integrated scattering cross section of an effective two-level emitter with radiative width $N\Gamma_0$:

$$\sigma(\delta) = \sigma \frac{(N\Gamma_0)^2}{(N\Gamma_0)^2 + 4\delta^2}. \quad (\text{F1})$$

Integrating over the detuning yields:

$$\langle \sigma \rangle = \int \sigma(\delta) d\delta = \frac{\pi}{2} N\Gamma_0 \sigma. \quad (\text{F2})$$

Likewise, the extinction cross section under coherent driving,

$$\sigma_{\text{ext}}(\delta) \equiv \sigma_{\text{sc}} + \sigma_{\text{abs}} = \sigma \frac{N\Gamma_0 (N\Gamma_0 + \Gamma_{\text{D}} + \Gamma_{\text{T}})}{(N\Gamma_0 + \Gamma_{\text{D}} + \Gamma_{\text{T}})^2 + 4\delta^2}, \quad (\text{F3})$$

satisfies

$$\int_{-\infty}^{\infty} \sigma_{\text{ext}}(\delta) d\delta = \frac{\pi}{2} N\Gamma_0 \sigma, \quad (\text{F4})$$

showing that detuning integration removes any dependence on Γ_{D} and Γ_{T} from the overall extinction (excitation) probability.

The corresponding detuning-integrated absorption cross section is then:

$$\langle \sigma_{\text{abs}} \rangle = \frac{\Gamma_{\text{D}} + \Gamma_{\text{T}}}{N\Gamma_0 + \Gamma_{\text{D}} + \Gamma_{\text{T}} + \Gamma_{\text{D}}\Gamma_0/\Gamma_{\text{T}}} \langle \sigma \rangle, \quad (\text{F5})$$

which reproduces the same functional dependence as obtained for incoherent illumination (upon the photon-flux identification above).